Comparison of Correlation-Based OFDM Radar Receivers

Steven Mercier, Stéphanie Bidon, Damien Roque, Cyrille Enderli

▶ **To cite this version:**

Steven Mercier, Stéphanie Bidon, Damien Roque, Cyrille Enderli. Comparison of Correlation-Based OFDM Radar Receivers. IEEE Transactions on Aerospace and Electronic Systems, 2020, 56 (6), pp.4796-4813. 10.1109/TAES.2020.3003704 . hal-03043178

HAL Id: hal-03043178
https://hal.science/hal-03043178v1

Submitted on 7 Dec 2020

HAL is a multi-disciplinary open access archive for the deposit and dissemination of scientific research documents, whether they are published or not. The documents may come from teaching and research institutions in France or abroad, or from public or private research centers.

L'archive ouverte pluridisciplinaire **HAL**, est destinée au dépôt et à la diffusion de documents scientifiques de niveau recherche, publiés ou non, émanant des établissements d'enseignement et de recherche français ou étrangers, des laboratoires publics ou privés.

Open Archive Toulouse Archive Ouverte (OATAO)

OATAO is an open access repository that collects the work of some Toulouse researchers and makes it freely available over the web where possible.

This is an author's version published in: https://oatao.univ-toulouse.fr/25917

Official URL: https://doi.org/10.1109/TAES.2020.3003704

To cite this version :

Mercier, Steven and Bidon, Stéphanie and Roque, Damien and Enderli, Cyrille Comparison of Correlation-Based OFDM Radar Receivers. (2020) IEEE Transactions on Aerospace and Electronic Systems. ISSN 0018-9251

Any correspondence concerning this service should be sent to the repository administrator: tech-oatao@listes-diff.inp-toulouse.fr

Comparison of Correlation-Based OFDM Radar Receivers

Steven Mercier, *Student Member, IEEE,* Stéphanie Bidon, *Senior Member, IEEE,*
Damien Roque, *Senior Member, IEEE,* and Cyrille Enderli

***Abstract*—Various correlation-based receivers have been proposed in passive bistatic and active monostatic radar exploiting orthogonal frequency-division multiplexing (OFDM) communications signals, but too little has been dedicated to establishing their relations and advantages over each other. Accordingly, this paper provides an analytical comparison of the common filters in such waveform sharing scenarios, along with a performance analysis regarding three criteria: computational complexity, signal-to-interference-plus-noise-ratio and resilience to ground clutter. The last two especially assess the possible detrimental effects of the random sidelobes (or pedestal) induced by the data symbols in the range-Doppler map. Although simulations show that none of the filters performs unanimously better, the ones employing circular correlations globally evidence attractive results.**

***Index Terms*—Active monostatic radar-communications (RadCom), orthogonal frequency-division multiplexing (OFDM), passive bistatic radar (PBR), random sidelobes, waveform sharing**

I. Introduction

As the electromagnetic spectrum congestion gets increasingly tangible, investigations for making a more efficient use of the radio frequencies are flourishing [1]–[4]. Especially, since communications and radar systems hold a significant part of this resource, they are naturally in the spotlight of this ongoing research. Among the variety of proposed solutions has emerged the idea of exploiting a single waveform to fulfill both functions simultaneously.

Passive bistatic radar (PBR) has for instance gained a lot of interest over the last decades with the proliferation of broadcast transmitters [5]–[7] and cellular networks [8], [9]. These readily available communications transmitters can indeed be exploited as illuminators of opportunity for low-cost and covert radar sensing. The joint waveform solution has also been suggested for RadCom, namely monostatic active radar and communications [10]–[12]. In this case, whether the waveform is specifically co-designed to this dual usage or simply exploited to transcend its initial purpose (either sensing or communicating), it would additionally benefit hardware integration and thereby save other valuable resources such as weight, volume and energy.

In both PBR and RadCom, a candidate that keeps drawing attention is the orthogonal frequency-division multiplexing (OFDM) waveform. OFDM indeed relies on low-complexity transmitters and receivers based on fast Fourier transforms (FFT) while being robust against channel's frequency selectivity [13]. Accordingly, it is now part of an increasing number of communications systems such as digital audio broadcasting (DAB) [14], terrestrial digital video broadcasting (DVB-T) [15] or long term evolution (LTE) [16], and therefore provides a substantial coverage for PBR [7], [9], [17]. OFDM has also demonstrated its capability for RadCom systems, for instance in radar networks [18], [19] and intelligent transportation systems such as vehicles [20], [21].

Still, in these applications, the OFDM waveform is initially intended for communications. As such, it bears sequences of data symbols to convey a message, as well as periodic elements such as pilots and cyclic prefixes (CP) to ease its recovery [13]. For a radar receiver, these features are however quite unconventional and result in non classical (potentially detrimental) effects in range-Doppler maps obtained via correlation-based algorithms.

The problem is theoretically even more exacerbated in the case of PBR since the transmitted signal employed in the correlation is *a priori* unknown. Interestingly enough, though, when exploiting digitally modulated waveforms under mild conditions, perfect demodulation and remodulation of the baseband transmitted signal can be achieved, and is therefore generally presumed in OFDM PBR [17], [22]. In this context, correlation-based OFDM radar receivers are possibly the same in PBR and in RadCom; hence their literature should be pooled.

In fact, several correlation-based OFDM radar receivers have been independently proposed by one community or the other so far (*e.g.*, see [7], [17], [23], [24]), but little has been devoted to unifying the whole framework. As such, despite some preliminary work [25], [26], receivers have never been clearly related to one another, and their performance have rarely been assessed on well-defined metrics, or else in restrictive scenarios. Particularly, the disturbance induced by the data symbols in the range-Doppler map, referred to as *random sidelobes*, or *pedestal*, which is commonly considered as a stochastic interference component adding up to thermal noise, has only been quantified for two filters while assuming delays up to the CP duration [26]. Furthermore, the behavior of these linear receivers in presence of ground clutter have mostly—but not exclusively (*e.g.*, see the recent work [27])—been observed in terrestrial PBR scenarios, in which clutter is mainly static and quite localized in range.

In this paper we describe and compare the most commonly

S. Mercier, S. Bidon and D. Roque (firstname.lastname@isae-supaero.fr) are with ISAE-SUPAERO, Université de Toulouse, France.

C. Enderli (cyrille-jean.enderli@fr.thalesgroup.com) is with Thales DMS, Élancourt, France.

The work of Steven Mercier is supported by DGA/MRIS under grant 2017.60.0005 and Thales DMS.

encountered correlation-based OFDM radar receivers, in both PBR and RadCom literature. Our contribution is to motivate and analytically relate the different receivers, but also to provide a performance analysis based on three criteria: (i) computational complexity; (ii) signal-to-interference-plus-noise-ratio (SINR), where the interference term stands for the aforementioned pedestal component; closed-form expressions are especially developed for any target in the range-Doppler map including ranges exceeding the CP; (iii) resilience to ground clutter, exemplified in a simulated RadCom forward-looking airborne scenario where it is highly extended. Subsequent clutter mitigation and target detection stages are however not carried out in this work.

The remainder of this paper is organized as follows. In Section II, the joint radar-communications OFDM transmitter and single-scatterer radar channel are first described. The various correlation-based radar receivers from the literature are then introduced, particular attention being paid to their relation with each other. Section III derives the output range-Doppler maps expressions, taking into account the aforementioned symbols-induced pedestal. Section IV compares the performance of the radar receivers in terms of complexity, SINR and resilience to clutter, for a certain variety of scenarios. Finally, concluding remarks and prospects are compiled in Section V.

Notation:

We use $\mathbf{Z}$ for the set of integers. $\mathcal{I}_N$ and $\bar{\mathcal{I}}_N$ denote the finite sets $\{0,\dots,N-1\}$ and $\{-N,\dots,-1\}$, respectively, and $\setminus$ the set difference. $\mathbb{E}\{\cdot\}$ is the expectation operator, $\|\cdot\|$ the ℓ_2-norm and sgn is the *signum* function anywhere but in 0 where we set $\mathrm{sgn}(0) \triangleq 1$. The so-called Dirichlet kernel is defined as:

$$\mathcal{D}_N(u) \triangleq \frac{1}{N}\sum_{n=0}^{N-1} e^{j2\pi\frac{n}{N}u}.$$

II. OFDM RADAR SYSTEM MODEL

In this paper, although the OFDM waveform is jointly used for radar and communications, we mainly focus on the radar system model. We refer for instance to [13] for the well-covered OFDM communication part.

A. Joint OFDM transmitter

The OFDM transmitter sends frames of M consecutive blocks—or sweeps—using simultaneously K orthogonal subcarriers over the bandwidth B, to a remote OFDM receiver.

Within a frame, each subcarrier k of a block m conveys a complex elementary symbol $c_{k,m}$, being either data, pilot or null, according to the exploited system (*e.g.*, DAB [14], DVB-T [15], LTE [16], etc.). To anticipate multipath effects in the channel, each block m is prefixed by a replica of its last $\Delta \in \mathcal{I}_K$ samples, prior to transmission. This portion of the block is referred to as the cyclic prefix (CP), in contrast to the so-called useful part.

Provided that $K \gg 1$, the baseband expression of a transmitted OFDM frame critically sampled at rate B is therefore [28]

$$s[p] = \sum_{m=0}^{M-1}\left(\frac{1}{\sqrt{K}}\sum_{k=0}^{K-1} c_{k,m}e^{j2\pi\frac{k}{K}(p-mL)}\right) g[p-mL] \quad (1)$$

where g denotes the rectangular pulse, arbitrarily chosen here to ensure $\|g\|^2 = K$, namely

$$g[p] \triangleq \begin{cases}\sqrt{\frac{K}{L}} & \text{if} \quad p \in \mathcal{I}_L \\ 0 & \text{otherwise}\end{cases} \quad (2)$$

and $L \triangleq K+\Delta$ is the extended block length, or indifferently, the pulse repetition interval (PRI). It is worth recalling that a longer CP comes at the cost of a reduced transmission's spectral efficiency $\eta \propto K/L$.

B. Radar channel

In the rest of the paper, we adopt the formalism used in monostatic radar scenario though it could be easily replaced by that of PBR (*e.g.*, bistatic range instead of range).

While propagating in the direction of the communication receiver at the speed of light c, the transmitted narrowband OFDM signal (1) is partly backscattered towards the radar receiver by a single point target[1] deemed to be characterized by:

- a zero-mean complex amplitude α;
- a radial velocity v inducing a simple frequency shift on s equal to $F_\mathrm{D} \triangleq 2vF_\mathrm{c}/c \ll B$ with F_c the transmitter's carrier frequency;
- an unambiguous range $R_0 = l_0\delta_\mathrm{R}$, with $l_0 \in \mathcal{I}_K$ the so-called range gate and $\delta_\mathrm{R} \triangleq c/(2B)$ the radar range resolution.

We especially assume these parameters to be constant during a frame. Therefore, as we ignore clutter for now, the baseband signal at the input of the radar receiver critically sampled at B is given by [28]

$$r[p] = \alpha\exp(j2\pi f_\mathrm{D}p/L)s[p-l_0] + w[p] \quad (3)$$

where $f_\mathrm{D} \triangleq F_\mathrm{D}L/B$ denotes the target's normalized Doppler frequency, and w the thermal noise modeled as a zero-mean white circular Gaussian contribution, with variance σ^2.

Note that after proper synchronization and direct path removal, a similar signal model is obtained on the surveillance channel of a bistatic radar receiver (*e.g.*, see [17, Eq. (5)]).

C. Correlation-based OFDM radar receiver

Whether it is considered in the monostatic or the bistatic topology, signal (3) is then usually processed to obtain an estimate of the illuminated radar scene in the range-Doppler domain. To that end, several correlation-based receivers have been proposed so far. Herein we recall the motivations and definitions of those mostly encountered in the OFDM PBR and RadCom literature. They are intentionally normalized so as to ensure the same peak power for a target at zero range and zero Doppler, when considering unit-variance data symbols. Names, acronyms and output notations we give to these filters are summarized in Table I.

[1]Extension to multitarget is straightforward but not treated here for the sake of clarity.

TABLE I
MAIN CORRELATION-BASED OFDM RADAR RECEIVERS

Full name	Acronym	Notation
Matched filter	MF	$\chi^{(r,s)}$
Proximate matched filter	PMF	$\widetilde{\chi}^{(r,s)}$
Proximate matched filter after CP-removal	PMF-CP	$\widetilde{\chi}^{(\check{r},s)}$
Proximate matched filter with circular correlation	PMF-CC	$\widetilde{\chi}^{(\check{r},s_0)}$
Reciprocal filter	RF	$\chi^{(r,\bar{s})}$
Proximate reciprocal filter	PRF	$\widetilde{\chi}^{(r,\bar{s})}$
Proximate reciprocal filter after CP-removal	PRF-CP	$\widetilde{\chi}^{(\check{r},\bar{s})}$
Proximate reciprocal filter with circular correlation (symbol-based)	PRF-CC	$\widetilde{\chi}^{(\check{r},\bar{s}_0)}$

1) Matched filtering approaches: Since range-Doppler processing is usually a prior step to radar detection, conventional approaches based on matched filtering have naturally been suggested.

a) Matched filter (MF): The filter matched to r in (3) is known to be the optimum linear filter in terms of signal-to-noise-ratio (SNR) at the coordinates of the target, namely (l_0, f_{D}). Presuming the coherent processing interval (CPI) is equal to the OFDM frame length, the MF output is given by the cross-correlation over LM samples[2] between Doppler shifted versions of r and a replica of the assumed known transmitted signal s, namely [7], [29]

$$\chi^{(r,s)}(l,\nu) \triangleq \frac{1}{\sqrt{KM}} \sum_{p=0}^{LM-1} r[p]s^*[p-l]e^{-j2\pi\nu p/L}. \quad (4)$$

However, to introduce the subsequent filters with more convenience, we rather rewrite it under the form

$$\chi^{(r,s)}(l,\nu) \triangleq \frac{1}{\sqrt{M}} \sum_{m=0}^{M-1} \chi_m^{(r,s)}(l,\nu)e^{-j2\pi\nu m} \quad (5)$$

where the function $\chi_m^{(r,s)}$ denotes the same cross-correlation, but this time computed over a single block m of the received signal r, *i.e.*, over L samples:

$$\chi_m^{(r,s)}(l,\nu) = \frac{1}{\sqrt{K}} \sum_{p=0}^{L-1} r[p+mL]s^*[p+mL-l]e^{-j2\pi\nu p/L}. \quad (6)$$

In fact, we will see in what follows that the main correlation-based OFDM radar receivers of the literature can be expressed through slight changes in (5)–(6).

b) Proximate matched filter (PMF): The high computational load of the MF (see Section IV-B) may be prohibitive in practice. Therefore, despite the integration loss incurred by such simplification (see Section IV-C), the MF is often approximated by ignoring the phase rotation due to the Doppler of the target within a block [22, Eq. (9)], [23]. In other words, the PMF reduces (6) to a single cross-correlation—or range compression—for each sweep m, prior to computing a Fourier transform over the sweeps:

$$\widetilde{\chi}^{(r,s)}(l,\nu) \triangleq \frac{1}{\sqrt{M}} \sum_{m=0}^{M-1} \chi_m^{(r,s)}(l,0)e^{-j2\pi\nu m}. \quad (7)$$

In practice, since the Doppler dimension is also discretized, an FFT algorithm is actually performed in (7), thereby decreasing drastically the receiver's complexity.

Notice that both the MF (5) and PMF (7) described so far are common radar receivers, regardless of the waveform. However, as it will be seen in the next Sections, in addition to thermal noise, an unconventional pedestal component, or random sidelobes, induced by the radar returns and involving the transmitted data symbols is susceptible to appear in the range-Doppler map. To limit the level of this interference, processings that take advantage of the OFDM structure have been advocated.

c) PMF after CP-removal (PMF-CP): One of these receivers consists in removing the CP from each block of the received signal r, prior to applying the PMF, yielding the PMF-CP receiver [7], [17]

$$\widetilde{\chi}^{(\check{r},s)}(l,\nu) \triangleq \frac{1}{\sqrt{M}} \sum_{m=0}^{M-1} \chi_m^{(\check{r},s)}(l,0)e^{-j2\pi\nu m} \quad (8)$$

where $\chi_m^{(\check{r},s)}$ is deduced from (6) by replacing the signal r with $\check{r}$, defined as

$$\check{r}[p] \triangleq \sqrt{\frac{L}{K}} r[p] \sum_{m_0 \in \mathbf{Z}} \check{g}[p-m_0L] \quad (9)$$

where $\check{g}$ is the conventional OFDM receive pulse-shape that fulfills the perfect symbol reconstruction condition given g [30, Eq. (6)], *viz*

$$\check{g}[p] \triangleq \begin{cases} \sqrt{\frac{L}{K}} & \text{if} \quad p \in \mathcal{I}_L \setminus \mathcal{I}_\Delta \\ 0 & \text{otherwise.} \end{cases} \quad (10)$$

Due to the CPs in the transmitted signal s, each function $\chi_m^{(\check{r},s)}(l,0)$ actually reduces on the range domain $l \in \mathcal{I}_\Delta$ to a circular correlation between

$$\boldsymbol{r}_m \triangleq [r[\Delta+mL],\ldots,r[L-1+mL]] \quad \text{and}$$
$$\boldsymbol{s}_m \triangleq [s[\Delta+mL],\ldots,s[L-1+mL]].$$

That way and as it will be evidenced in Section IV-C, if $\boldsymbol{r}_m$ is simply a circularly shifted version of $\boldsymbol{s}_m$, then thanks to the subcarrier orthogonality of the OFDM waveform, a limited—possibly null—pedestal is produced in the range bins $l \in \mathcal{I}_\Delta$. Such condition is especially met when the scatterer is static, with delay smaller than the CP duration.

[2]Given the received signal model (3), this implies discarding the last l_0 useful samples of r. In a realistic scenario where $M \gg 1$, the impact of such truncation is however negligible and will therefore be omitted in our development.

d) PMF with circular correlation (PMF-CC): Interestingly, and as suggested by [25], the latter achievable pedestal-limited region can be extended to the whole range domain of interest $l \in \mathcal{I}_K$ by fully circularizing the correlation in function $\chi_m^{(\check{r},s)}$ of the PMF-CP. This results in the PMF-CC receiver

$$\widetilde{\chi}^{(\check{r},s_0)}(l,\nu) \triangleq \frac{1}{\sqrt{M}} \sum_{m=0}^{M-1} \chi_m^{(\check{r},s_0)}(l,0) e^{-j2\pi\nu m} \tag{11}$$

where $\chi_m^{(\check{r},s_0)}(l,0)$ denotes the circular correlation between $\boldsymbol{r}_m$ and $\boldsymbol{s}_m$, as s_0 is the per-block circularized version of s, namely

$$s_0[p+mL] \triangleq \begin{cases} s[p+K+mL] & \text{if} \quad p \in \bar{\mathcal{I}}_{K-\Delta-1} \\ s[p+mL] & \text{if} \quad p \in \mathcal{I}_L. \end{cases}$$

Nonetheless, since the main interest of circular correlation lies in its efficient computability with an FFT algorithm, we prefer expressing it as

$$\chi_m^{(\check{r},s_0)}(l,0) = \frac{L}{K} \mathrm{FFT}_K^{-1}\left\{\mathrm{FFT}_K\{\boldsymbol{r}_m\} \odot \mathrm{FFT}_K^*\{\boldsymbol{s}_m\}\right\}[l], \quad l \in \mathcal{I}_K \tag{12}$$

with FFT_K a unitary FFT of size K and $\odot$ the Hadamard or element-wise product, and where, given (1) and (2)

$$\mathrm{FFT}_K^*\{\boldsymbol{s}_m\} = \sqrt{\frac{K}{L}} \boldsymbol{c}_m^* \quad \text{with} \quad \boldsymbol{c}_m \triangleq [c_{0,m}, \ldots, c_{K-1,m}]. \tag{13}$$

In plain English, (11)–(12)–(13) therefore mean that the PMF-CC basically: (i) estimates the time-frequency shifted elementary symbol in each subband of the received signal, as in a regular linear OFDM communication receiver; (ii) multiplies it by the conjugate of the (known) elementary symbol actually transmitted in that subband; (iii) computes a 2-dimensional FFT, transforming the subband-slow time domain into the range-Doppler domain of interest.

It is worth noting that the PMF-CC architecture can be easily extended to apply Doppler shifts multiples of the subcarrier spacing in (12) for compensating fast intra-block Doppler phase rotations and solving Doppler ambiguity [31]. This extension is no longer a rigorous proximate filter, though.

2) Reciprocal filtering approaches: Most of the previous correlation-based receivers have also been considered for reciprocal—in place of matched—filtering. The reciprocal filter (RF) aims at equalizing the spectrum of the transmitted signal [32]. Beyond its ability to attenuate the spurious peaks due to signal periodicities such as pilots (*e.g.*, see [22]), this zero-forcing-like technique has also been advocated to further reduce the aforementioned random sidelobes of strong returns observed with the conventional matched filtering approaches [25], [26], [33].

By construction of the OFDM waveform, reciprocal filtering simply consists in our context in replacing in (5)–(7)–(8)–(11) the replica of the transmitted signal s (or the substitute s_0) by the signal $\bar{s}$ (or $\bar{s}_0$) that conveys the sequence $\left\{1/c_{k,m}^*\right\}_{k,m}$ instead of $\{c_{k,m}\}_{k,m}$. One may then notice that:

- there is no difference between the matched and reciprocal strategies in the case of unit-variance phase-shift keying (PSK) constellations, as opposed for instance to amplitude-PSK (APSK) or quadrature amplitude modulations (QAM);
- the proximate reciprocal filter with circular correlation (PRF-CC), which was quite recently introduced in PBR under the acronyms MCC [25] and CHAD [26], actually corresponds to the so-called *symbol-based* processing proposed a few years earlier in the active radar literature [24].

The latter remark particularly emphasizes the need to unify the literature on OFDM radar, which is one of the purposes of this paper.

3) Hybrid approaches: Hybrid versions of the previous filters are also found in the OFDM radar literature. Particularly, in terrestrial PBR, the direct path and clutter are frequently rejected from the surveillance channel *via* orthogonal projection in the subband domain—reached out with the PMF-CC and PRF-CC approaches—for computational convenience. The signal is then transformed back into the range domain to apply a more conventional MF or PMF processing [7], [34]–[36]. It is nonetheless worth noticing that these techniques assume the absence of a significant clutter pedestal and have naturally been proved defective otherwise [37]. Moreover, the improvement brought by stacking circular and linear correlations has *per se* not been discussed.

III. Correlation-based receivers outputs

Herein, we provide the outputs of the filters presented in Section II, namely the range-Doppler maps expressions, in absence of thermal noise w. While referring to Appendix A for the details of derivation, we sum up the results for the matched filtering approaches in (14a)–(14d). Their reciprocal counterparts are simply deduced by replacing the term $c_{k',m'}^*$ with $1/c_{k',m'}$ in each equation.

For the sake of compactness and to highlight the similarities between the expressions, we have introduced the pulse-ambiguity functions

$$A^{(g,g)}(l,f) \triangleq \frac{1}{K} \sum_{p=0}^{L-1} g[p] g^*[p-l] e^{j2\pi fp} \tag{15}$$

$$A^{(g,\check{g})}(l,f) \triangleq \frac{1}{K} \sum_{p=0}^{L-1} g[p] \check{g}^*[p-l] e^{j2\pi fp} \tag{16}$$

$$\text{MF} \quad \chi^{(r,s)}(l,\nu) \underset{M\gg 1}{\simeq} \alpha e^{j2\pi(f_\mathrm{D}-\nu)l_0/L} \sum_{k,m}\sum_{k',m'} c_{k,m}c^*_{k',m'}\Psi_{k',m,m',l,\nu}A^{(g,g)}\left(l-l_0+(m'-m)L, \frac{f_\mathrm{D}-\nu}{L}+\frac{k-k'}{K}\right) \tag{14a}$$

$$\text{PMF} \quad \widetilde{\chi}^{(r,s)}(l,\nu) \underset{M\gg 1}{\simeq} \alpha e^{j2\pi f_\mathrm{D} l_0/L} \sum_{k,m}\sum_{k',m'} c_{k,m}c^*_{k',m'}\Psi_{k',m,m',l,\nu}A^{(g,g)}_{\{l_0,\nu\}}\left(l-l_0+(m'-m)L, \frac{f_\mathrm{D}}{L}+\frac{k-k'}{K}\right) \tag{14b}$$

$$\text{PMF-CP} \quad \widetilde{\chi}^{(\check{r},s)}(l,\nu) \underset{M\gg 1}{\simeq} \alpha e^{j2\pi f_\mathrm{D} l_0/L} \sum_{k,m}\sum_{k',m'} c_{k,m}c^*_{k',m'}\Psi_{k',m,m',l,\nu}\dot{A}^{(\check{g},g)}_{\{l_0,\nu\}}\left(l-l_0+(m'-m)L, \frac{f_\mathrm{D}}{L}+\frac{k-k'}{K}\right) \tag{14c}$$

$$\text{PMF-CC} \quad \widetilde{\chi}^{(\check{r},s_0)}(l,\nu) \underset{M\gg 1}{\simeq} \alpha e^{j2\pi f_\mathrm{D} l_0/L} \sum_{k,m}\sum_{k',m'} c_{k,m}c^*_{k',m'}e^{j2\pi\nu(m-m')}\Psi_{k',m,m',l,\nu}A^{(g,\check{g})}\left(-l_0+(m'-m)L, \frac{f_\mathrm{D}}{L}+\frac{k-k'}{K}\right) \tag{14d}$$

$$\text{with} \quad \Psi_{k',m,m',l,\nu} = e^{j2\pi\frac{k'}{K}(l-l_0+(m'-m)L)}e^{j2\pi(f_\mathrm{D}-\nu)m}/\sqrt{KM}$$

as well as improper versions

$$A^{(g,g)}_{\{l_0,\nu\}}(l,f) \triangleq \frac{1}{K}\left(\sum_{p=0}^{L-l_0-1} g[p]g^*[p-l]e^{j2\pi fp} + e^{-j2\pi\nu}\sum_{p=L-l_0}^{L-1} g[p]g^*[p-l]e^{j2\pi fp}\right) \tag{17}$$

$$\dot{A}^{(\check{g},g)}_{\{l_0,\nu\}}(l,f) \triangleq \frac{1}{K}\left(\sum_{p=0}^{L-l_0-1} \check{g}[p+l_0]g^*[p-l]e^{j2\pi fp} + e^{-j2\pi\nu}\sum_{p=L-l_0}^{L-1} \check{g}[p+l_0-L]g^*[p-l]e^{j2\pi fp}\right). \tag{18}$$

We emphasize that the derived range-Doppler map expressions are valid for any target described in Section II-B. This contrasts with the restriction to targets below the CP (*i.e.*, $l_0 \in \mathcal{I}_\Delta$) that has been almost exclusively investigated in the OFDM radar literature so far. In this particular case, in (14d) we have

$$A^{(g,\check{g})}(-l_0+(m'-m)L,f) = e^{-j2\pi f l_0}A^{(g,\check{g})}(0,f)\delta_{m,m'} \tag{19}$$

while in (14c) we get, $\forall l \in \mathcal{I}_K$,

$$\dot{A}^{(\check{g},g)}_{\{l_0,\nu\}}(l-l_0+(m'-m)L,f) = e^{j2\pi f(l-l_0+(m'-m)L)}A^{(g,\check{g})}(-l+(m-m')L,f). \tag{20}$$

Accordingly, if the range observation is restricted to $l \in \mathcal{I}_\Delta$ as well, we can inject (19) into (20), to yield

$$\dot{A}^{(\check{g},g)}_{\{l_0,\nu\}}(l-l_0+(m'-m)L,f) = A^{(g,\check{g})}(-l_0+(m'-m)L,f)$$

thus proving that the PMF-CP (14c) and the PMF-CC (14d) (or indifferently, the PRF-CP and PRF-CC) are rigorously equivalent on the range domain $l \in \mathcal{I}_\Delta$. As a result, the performance comparison between the PMF-CP and the PRF-CC established in [26] (referred to as CAF and CHAD, respectively) eventually measures the advantage brought by the reciprocal filter PRF-CC over its matched counterpart PMF-CC for typical DVB-T signals in terms of pedestal level, when not exceeding the CP. As such, the remainder of this paper can be seen as a generalization of this performance comparison: to the full range domain of interest (*i.e.*, considering $l_0, l \in \mathcal{I}_K$); to other filters commonly used in the OFDM radar literature; and to alternate performance criteria.

IV. Performance comparison

In this Section, we compare the theoretical performance of the different filters of Table I regarding two common criteria: computational complexity and SINR. The behavior of the filters in presence of ground clutter is also examined on synthetic range-Doppler maps.

A. Preliminary assumptions

For the sake of simplicity, we assume in what follows that the complex symbols $c_{k,m}$ in (1) are only data. Although unrealistic from the communication viewpoint, assuming neither pilot nor null symbol in the transmitted signal s indeed allows us to: (i) compact the SINR expressions derived in Section IV-C; (ii) focus our complexity analysis of Section IV-B on the correlation-based receivers *per se*, as we can ignore the stages aimed at handling the ambiguities related to such symbols (*e.g.*, see [22]). The data symbols are especially presumed independent and uniformly drawn from a constellation that is proper [38] and that satisfies also $\mathbb{E}\left\{1/c_{k,m}\right\} = 0$ and $\mathbb{E}\left\{c_{k,m}/c^*_{k,m}\right\} = 0$, such as PSK, APSK or QAM. We denote $\sigma_c^2 \triangleq \mathbb{E}\left\{|c_{k,m}|^2\right\}$, $\sigma^2_{c^{-1}} \triangleq \mathbb{E}\left\{1/|c_{k,m}|^2\right\}$ and $\mu_{c^4} \triangleq \mathbb{E}\left\{|c_{k,m}|^4\right\}$.

Again, for simplicity, but without loss of generality, we assume in what follows that the Doppler dimension is also critically sampled (*i.e.*, ν is of the form $\nu = n/M$ with $n \in \mathcal{I}_M$), and that the target is perfectly on-grid with $n_0 \triangleq f_\mathrm{D}M \in \mathcal{I}_M$ denoting its Doppler bin index. We recall that we suppose $M \gg 1$ to ignore the effects of the truncation of r by the radar receivers.

B. Computational complexity

We report in Table II the number of complex operations required by each receiver to compute a range-Doppler map of size $K \times M$, along with a numerical application based on our realistic simulated scenario of Section IV-D in terms

TABLE II
COMPUTATIONAL COMPLEXITY OF THE MAIN CORRELATION-BASED OFDM RADAR RECEIVERS

	Complex multiplications	Complex additions	MACs in the S&A scenario (Table IV)
MF/RF	$LM(K+1)M$	$(LM-1)KM$	$4.53E10$
PMF/PRF	$(L+1/2\log_2(M))KM$	$(L-1+\log_2(M))KM$	$5.68E08$
PMF-CP/PRF-CP	$(K+1/2\log_2(M))KM$	$(K-1+\log_2(M))KM$	$5.05E08$
PMF-CC/PRF-CC	$(\log_2(K)+1+1/2\log_2(M))KM$	$(2\log_2(K)+\log_2(M))KM$	$8.95E06$

of multiply–accumulate operations (MACs). They have been counted assuming that:

- operations such as normalization, conjugation or CP removal can be neglected;
- divisions are equivalent to multiplications;
- linear correlations and partial circular correlations (*e.g.*, with the PMF-CP) are computed in the time domain;
- performing an FFT of size N requires $N/2\log_2(N)$ complex multiplications and $N\log_2(N)$ complex additions;
- complex additions and multiplications are worth 2 and 4 MACs, respectively.

First, comparing the first and second rows, we clearly notice that the Doppler-phase approximation introduced in (7) highly reduces the computational load of the radar receiver, as expected. The following rows then show us that the receiver's complexity additionally decreases as it exploits the structure of the OFDM waveform. The presence of numerous FFTs in the PMF-CC and PRF-CC receivers especially results in significant computational savings.

C. SINR performance

With the aim of defining an informative metrics for further radar detection, we derive hereafter the first two moments of the range-Doppler maps, generically denoted by χ. We emphasize that the latter are the filters responses to a single target *amid* white noise and not pure ambiguity functions.

1) First- and second-order moments: On the one hand, since it is assumed that the thermal noise is zero-mean and that $\mathbb{E}\{\alpha\}=0$, we straightforwardly obtain $\mathbb{E}\{\chi[l,n]\}=0$.

On the other hand, we show in Appendices B and C that the power $\mathbb{E}\left\{|\chi[l,n]|^2\right\}$ can be split into[3]

$$\mathbb{E}\left\{|\chi[l,n]|^2\right\} = P_{\mathrm{t}}^{(\chi)}[l,n] + P_{\mathrm{i}}^{(\chi)}[l,n] + P_{\mathrm{w}}^{(\chi)} \qquad (21)$$

where each term can be easily identified for each filter from the expressions summed up in (26a)–(27d):

- $P_{\mathrm{t}}^{(\chi)}[l,n] \propto KM\left|\mathcal{D}_K(l-l_0)\right|^2\left|\mathcal{D}_M(n_0-n)\right|^2$ the target's signature power component;
- $P_{\mathrm{i}}^{(\chi)}[l,n]$ the so-called pedestal (or random sidelobes) power component;
- $P_{\mathrm{w}}^{(\chi)} \propto \sigma^2$ the post-processing thermal noise power.

[3]Although it is not developed here for the sake of compactness, it can actually be shown with the same procedure as used in Appendices B and C that the covariance matrix, abusively denoted $\mathbb{E}\{\chi[l,n]\chi^*[l',n']\}$, is diagonal (*i.e.*, $\mathbb{E}\{\chi[l,n]\chi^*[l',n']\}=0$ for $[l',n']\neq[l,n]$).

Although $P_{\mathrm{t}}^{(\chi)}[l,n]$ and $P_{\mathrm{w}}^{(\chi)}$ are usual in conventional radar, it is worth noticing that:

- the target peak $P_{\mathrm{t}}^{(\chi)}[l_0,n_0]$ may incur a loss monitored by a pulse-ambiguity squared-modulus term[4]. This integration loss can be attributed to either or both: (i) the uncompensated Doppler phase within a pulse, as for the so-called proximate filters (see (26b)–(26d) and (27b)–(27d)); (ii) a delay higher than the CP duration leading to block mismatching in circular correlations, as for the PMF-CC and PRF-CC (see (26d) and (27d));
- the post-processing noise power $P_{\mathrm{w}}^{(\chi)}$ endures an increase by factor L/K when removing the CP from the blocks of the received signal r, as for the PMF-CP, PMF-CC and their reciprocal counterparts (see (26c)–(26d) and (27c)–(27d)).

For its part, the pedestal power component $P_{\mathrm{i}}^{(\chi)}[l,n]$ is specifically related to the presence of random elements (*i.e.*, the data symbols $c_{k,m}$) in the transmitted signal (1). It is worth underlining that since we assume the data symbols to be known, they could in theory be used to remove the pedestal of each scatterers (*e.g.*, see [39]). This strategy is out of the scope of this work. Instead, we consider data symbols as a stochastic component in the range-Doppler map challenging detection performance.

In this context, we observe that contrary to what is broadly admitted in the literature, the pedestal in OFDM radar is not systematically white in the range-Doppler domain as its power may depend on the cell under test $[l,n]$. Actually, from (26d) and (27d), whiteness is verified only for the PMF-CC and PRF-CC. Otherwise, its power globally increases with the distance between the range-Doppler bin $[l,n]$ and that of the target $[l_0,n_0]$.

Besides and as expected by design, depending on the filtering approach (namely matched or reciprocal), we observe that the three power components involve different order statistics of the data symbols. This point is examined in more details hereafter.

2) Post-processing SINR: Detection performance of conventional radar systems are highly determined by the post-processing SNR metrics [40]. For our OFDM-based radar system, to additionally account for the pedestal component,

[4]The modulus of the pulse-ambiguity functions (15)–(18) are indeed bounded from above by 1.

TABLE III
WAVEFORM AND CHANNEL PARAMETERS FOR SINR SIMULATIONS

Parameter	Variable	Value
Number of subcarriers	K	128
Cyclic prefix length	Δ	16
Number of blocks	M	32
Constellation	$c_{k,m}$	QPSK
Target power	$\mathbb{E}\{\lvert\alpha\rvert^2\}$	0 dBW
Input noise power	σ^2	0 dBW

we rather define a post-processing SINR as

$$\mathrm{SINR}_{\chi}[l,n] \triangleq \frac{P_{\mathrm{t}}^{(\chi)}[l_0,n_0]}{P_{\mathrm{i}}^{(\chi)}[l,n]+P_{\mathrm{w}}^{(\chi)}}, \quad [l,n]\neq[l_0,n_0]. \tag{22}$$

Notice that the impacts of each filter on the different power components of (21) are therefore jointly quantified here, unlike in [26].

a) QPSK modulation: Let us first assume the use of a unit-variance QPSK modulation, so that the matched (26) and reciprocal (27) filtering approaches are equivalent. The SINR obviously highly depends on the pulse-ambiguity functions (15)–(18) and on the relative position that is observed in the range-Doppler map. Consequently, we consider various target scenarios and display in Figs. 1–3 different Doppler cuts of the post-processing SINRs. For each cut, the theoretical SINRs computed with (22), in solid lines, are represented along with the results obtained through Monte-Carlo simulations, in markers, to validate our derivations. The waveform and channel parameters used for these simulations are provided in Table III.

The target scenario of Fig. 1 is representative of the best situation for the PMF-CC. The target is in fact static with a range gate $l_0 \leq \Delta$, so that no pedestal is produced by the processing [28]. Therefore, despite its increased noise level by factor $L/K = -0.51$ dB, as evidenced in the first range bins of Fig. 1a, the PMF-CC outperforms the other filters in the rest of the range-Doppler map (*e.g.*, see the other range bins in the same figure, or the cut of Fig. 1b), including the MF and PMF. Indeed, although the latter achieve the highest SINR value, they eventually suffer from the growth of their pedestal power in line with $|l-l_0|$ and/or $|n-n_0|$. Especially, since the target is static here, attempting to compensate the nonexistent rotating Doppler phase within each block even seems to be detrimental for the MF, as hinted by Fig. 1b. Finally, in both Doppler cuts, the PMF-CP exhibits the same SINR as the PMF-CC on the first Δ range bins, as expected by design.

In Fig. 2, the former target is now assumed to move with a non-negligible velocity. As a result, the 3 proximate filters induce both an integration loss on their target peak and a pedestal rise (see the pulse-ambiguity squared-modulus terms in (26b)–(26c)–(26d)), yielding a degraded SINR compared to Fig. 1. In contrast, the MF still performs globally well. In range-Doppler bins distant from that of the target, it nonetheless once again gets outpaced by the uniformly-performing PMF-CC.

Fig. 3 finally depicts the case where the target is moving while being far beyond the CP. Filters globally perform the same as in Fig. 2, except the PMF-CC which now incurs a major integration loss jointly imputable to the significant target's Doppler frequency—as in the previous situation—*and* CP overshooting.

b) Amplitude modulations: Now let us consider the case of amplitude modulations—still assumed to have unit variance, by convention—and examine the impact on the SINR of the reciprocal strategy with respect to the usual matched approach. After few rearrangements, we show that the SINR ratio between the RF and MF boils down to (23). Since only the pulse-ambiguity squared-modulus terms change when considering the other filters, the following remarks hold as well.

- In noise-dominated scenarios such that $\sigma^2 \geq \mathbb{E}\{\lvert\alpha\rvert^2\}$ we get[4]:

$$\frac{\mathrm{SINR}_{\chi^{(r,\bar{s})}}[l,n]}{\mathrm{SINR}_{\chi^{(r,s)}}[l,n]} \leq \frac{\mu_{c^4}}{\sigma^2_{c^{-1}}}, \quad [l,n]\neq[l_0,n_0]. \tag{24}$$

  This upper bound is basically the ratio between the power of the absolute square and the mean of the inverse absolute square of the data symbols. For classical QAM modulations, it is lower than 1 and declines as the constellation size increases, as depicted in Fig. 4. Matched filtering approaches are therefore undoubtedly preferable in these scenarios.
- In presence of a highly reflective scatterer, *i.e.*, at least when $\sigma^2 < \mathbb{E}\{\lvert\alpha\rvert^2\}$, the analysis becomes trickier as the pulse-ambiguity squared-modulus terms vary with respect to either or both the target's and observation's parameters, $[l_0,n_0]$ and $[l,n]$, respectively. As such, the SINR of the reciprocal strategies may appear locally better around the target peak while performing poorly in the rest of the range-Doppler domain. Nonetheless, the case PRF-CC vs PMF-CC is easier to treat as they only depend on $[l_0,n_0]$ (*e.g.*, see [26]).

D. Behavior in presence of ground clutter

We assume from now on that a ground clutter component r_{c} is present in the received signal r, thereby adding to the initial model (3). Hereafter we describe its model and observe its impact on the filters outputs in a simulated scenario.

1) Clutter model: We model ground clutter as statistically independent patches, spreading in both range and azimuth dimensions. More specifically, at each range $R_{0_{i_{\mathrm{c}}}} = i_{\mathrm{c}}\delta_{\mathrm{R}}$ with $i_{\mathrm{c}} \in \mathcal{I}_{I_{\mathrm{c}}}$, we assume N_{c} equally spaced patches around the radar, characterized by

- a complex amplitude $\rho_{i_{\mathrm{c}},n_{\mathrm{c}}}$;
- a nominal Doppler frequency $F_{\mathrm{D}_{i_{\mathrm{c}},n_{\mathrm{c}}}} \ll B$;

so that the corresponding baseband received signal critically sampled at rate B is, as for targets, of the form

$$r_{\mathrm{c}}[p] = \sum_{i_{\mathrm{c}}=0}^{I_{\mathrm{c}}-1}\sum_{n_{\mathrm{c}}=0}^{N_{\mathrm{c}}-1} \rho_{i_{\mathrm{c}},n_{\mathrm{c}}} \exp(j2\pi f_{\mathrm{D}_{i_{\mathrm{c}},n_{\mathrm{c}}}} p/L) s[p-i_{\mathrm{c}}] \tag{25}$$

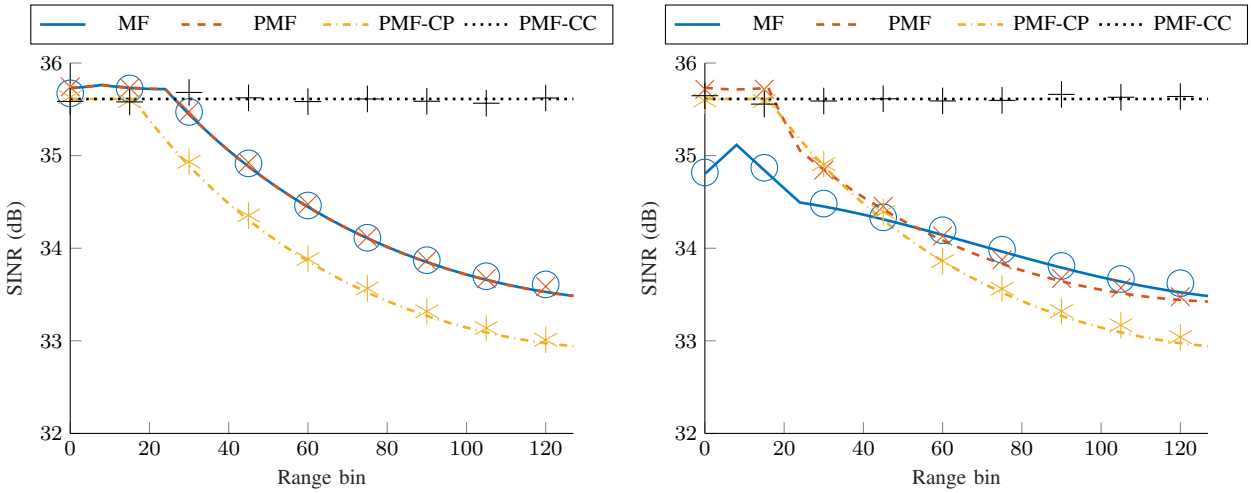

(a) Cut at $n = 1$ (b) Cut at $n = M/2 - 1$

Fig. 1. SINR Doppler cuts for target at $[l_0, n_0] = [\Delta/2, 0]$ (*i.e.*, target prior to the CP, static)

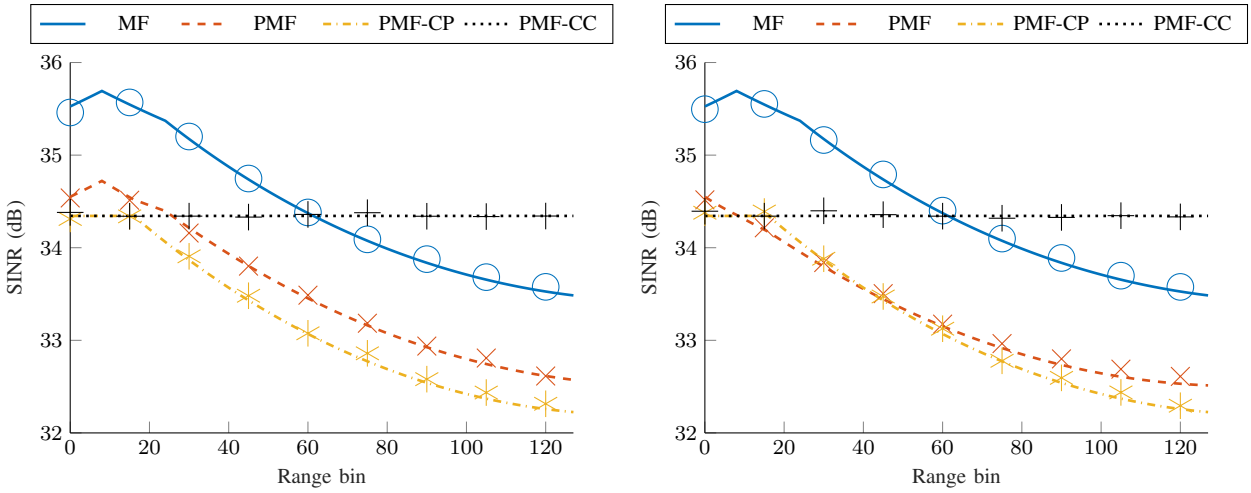

(a) Cut at $n = 1$ (b) Cut at $n = M/2 - 1$

Fig. 2. SINR Doppler cuts for target at $[l_0, n_0] = [\Delta/2, M/4]$ (*i.e.*, target prior to the CP, with Doppler close to 22 % of the subcarrier spacing)

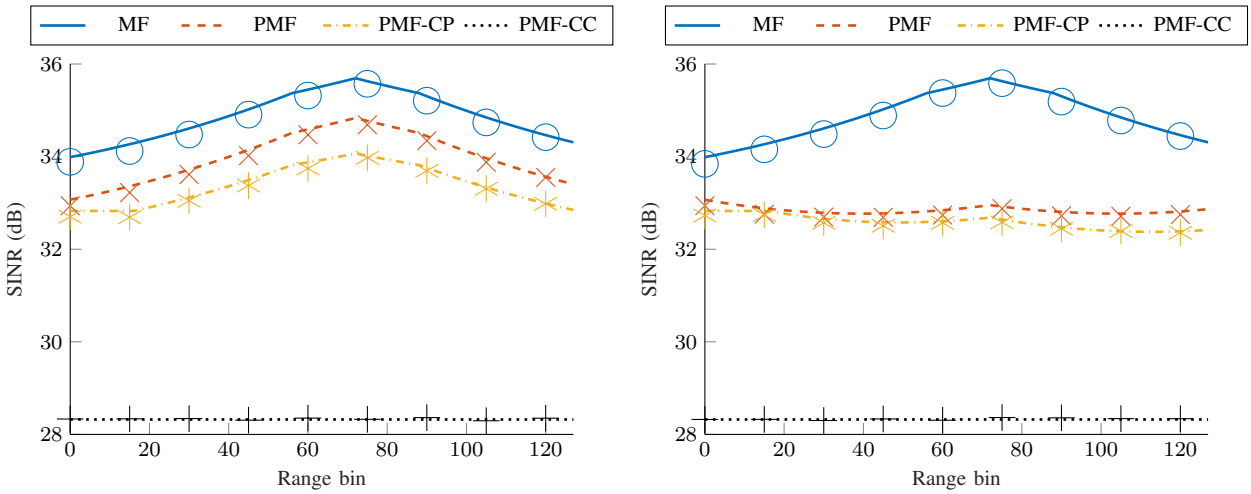

(a) Cut at $n = 1$ (b) Cut at $n = M/2 - 1$

Fig. 3. SINR Doppler cuts for target at $[l_0, n_0] = [L/2, M/4]$ (*i.e.*, target exceeding the CP by a factor 4.5, with Doppler close to 22 % of the subcarrier spacing)

$$\frac{\text{SINR}_{\chi^{(r,\bar{s})}}[l,n]}{\text{SINR}_{\chi^{(r,s)}}[l,n]} = \frac{1}{\sigma^2_{c^{-1}}} + \frac{\mu_{c^4}-1}{\sigma^2_{c^{-1}}} \frac{\left|A^{(g,g)}\left(l-l_0,\frac{n_0-n}{LM}\right)\right|^2}{\sum_{k'\neq 0}\left|A^{(g,g)}\left(l-l_0,\frac{n_0-n}{LM}+\frac{k'}{K}\right)\right|^2+\sum_{k'}\left|A^{(g,g)}\left(l-l_0-\text{sgn}(l-l_0)L,\frac{n_0-n}{LM}+\frac{k'}{K}\right)\right|^2+\frac{\sigma^2}{\mathbb{E}\{|\alpha|^2\}}}. \tag{23}$$

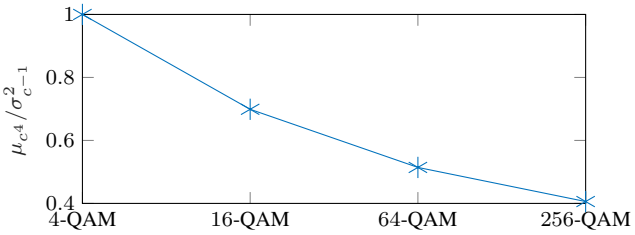

Fig. 4. Ratio $\mu_{c^4}/\sigma^2_{c^{-1}}$ for usual QAM modulations.

with $f_{\text{D}_{i_c,n_c}} \triangleq F_{\text{D}_{i_c,n_c}} L/B$ and where $P_{\rho_{i_c,n_c}} \triangleq \mathbb{E}\left\{|\rho_{i_c,n_c}|^2\right\}$ is computed from the radar equation for area clutter [41].

2) Simulation: The impact of ground clutter on the different correlation-based OFDM processings recalled in this paper has already been largely observed in terrestrial PBR. Since clutter returns are mainly static and below the CP duration in these scenarios, the subband domain (especially through the PRF-CC) is usually advocated to naturally limit its pedestal level as evidenced in Fig. 1 (*e.g.*, see [25], [26]). As a supplement to the existing work, we therefore examine in the following the impact of a more spread clutter, encountered for instance in RadCom airborne scenarios. The parameters used for the simulation are provided in Table IV. Note that a unit-variance QPSK modulation is assumed here, so that the matched and reciprocal strategies are once again equivalent.

Consider an active forward looking OFDM radar placed on an unmanned combat aerial vehicle (UCAV) for simultaneous communication and Sense & Avoid (S&A). The RadCom system operates at the carrier frequency $F_\text{c} = 5$ GHz, over a bandwidth of $B = 10$ MHz. The platform is at the altitude $H_\text{p} = 550$ m, moving horizontally at the speed $v_\text{p} = 120$ m/s. The transmit and receive antennas are positioned orthogonally to the platform motion. They are identical perfect uniform rectangular arrays composed of 8×4 half-wavelength spaced elements having cosine patterns and no backlobes. They are steering into the direction[5] $(\phi_{\text{max}}, \theta_{\text{max}}) = (0°, 10°)$ where they achieve their maximum gain $G_{\text{RX}_{\text{max}}} = G_{\text{TX}_{\text{max}}} \simeq 20.0$ dBi. Moreover, their 3-dB azimuthal and elevation beamwidths are $\Delta\phi \simeq 25.7°$ and $\Delta\theta \simeq 12.8°$, respectively.

Assuming a flat-earth model, the static ground clutter patch (i_c, n_c) has the Doppler frequency $F_{\text{D}_{i_c,n_c}} = 2v_\text{p}F_\text{c}\cos(\theta_{i_c})\sin(\phi_{n_c})/c$ with $\theta_{i_c} = \arccos\left(\sqrt{1-(H_\text{p}/R_{0_{i_c}})^2}\right)$ being its elevation angle, and ϕ_{n_c} its azimuth angle. Besides, it is assumed to follow a circularly-symmetric complex normal distribution, namely $\rho_{i_c,n_c} \sim \mathcal{CN}(0, P_{\rho_{i_c,n_c}})$. A constant gamma model is used to compute the area reflectivity of each patch [41], with

[5] $(\phi_{\text{max}}, \theta_{\text{max}})$ must change over time to cover the 220° azimuthal and 30° elevation apertures required for S&A [42].

TABLE IV
UCAV SENSE & AVOID SIMULATION PARAMETERS

Parameter	Variable	Value
Platform altitude	H_p	550 m
Platform velocity	v_p	120 m/s
Carrier frequency	F_c	5 GHz (C-band)
Antennas maximum gain	$G_{\text{RX}_{\text{max}}} = G_{\text{TX}_{\text{max}}}$	20.0 dBi
Antennas beamwidth	$(\Delta\phi, \Delta\theta)$	$(25.7°, 12.8°)$
Antennas direction	$(\phi_{\text{max}}, \theta_{\text{max}})$	$(0°, 10°)$
Various system losses	L_{syst}	5 dB
Bandwidth	B	10 MHz
Transmitted power	P_s	10 W
Number of subcarriers	K	1024
Cyclic prefix length	Δ	128
Number of blocks	M	80
Constellation	$c_{k,m}$	QPSK
Input noise power	σ^2	-130 dBW
Gamma	γ	-3 dB

$\gamma = -3$ dB. In this simulation, we have set $N_\text{c} = 360$ and $I_\text{c} = 2K$, so that clutter exceeds by far the CP.

The target is assumed to be an airliner just taking-off, at altitude 96 m, distance $R_0 = 2325$ m, with a radar cross section of 100 m^2 and a radial velocity of $v = 35.8$ m/s thereby respecting the required 20 s of advanced warning for S&A [42]. The white Gaussian noise w is simulated with input power $\sigma^2 = -130$ dBW. The resulting range-Doppler maps after platform velocity compensation are depicted in Fig. 5. For information, the CP range is symbolized with a horizontal blue line, and a magnification is made on the target area.

As intended, we observe that the clutter main contribution is highly extended in both range and velocity. Besides, its pedestal is white only with the PMF-CC (Fig. 5d), as justified in Section IV-C1. More importantly, one may notice that its level is substantially lower at the output of the PMF-CC, compared to the others. With this filter, the pedestal induced by the clutter scatterers below the CP duration is indeed greatly prevented. Concomitantly, the target peak power measured for the PMF-CC is quite close to that of the other range-Doppler maps, since the target does not significantly exceed the CP here. It results that this filter seems quite favorable for detection in such scenario, although a more in-depth analysis would be required to rigorously conclude, particularly as the

pedestal might not be normally distributed [28]. We still notice that the average pedestal level exceeds -110 dB for all filters, that is roughly 20 dB more than the theoretical post-processing white noise power. Such interference level, in complement to the clutter ridge itself, would therefore cause severe degradations in the radar performance and need to be further handled, as attempted for instance in [37].

V. Conclusion

In this paper, we have proceeded with a comparison of the main correlation-based radar receivers encountered in the joint radar-communications OFDM literatures of PBR and RadCom. The filters have first been compared from an analytical point of view, with particular emphasis put on the commonalities and differences between one another. Overlapping processings have especially been evidenced between PBR and RadCom authors, thereby justifying our attempt to unify this framework. The filters have then been compared *via* simulations in terms of performance. Particularly, in the prospect of target detection, a SINR metrics has been defined in the output range-Doppler maps. It accounts for the processing integration losses as well as their tolerance to noise, and to the so-called target's pedestal owing to the presence of data symbols into the dual-function OFDM signal. A complexity analysis has also been carried out, and the overall impact of strong extended clutter, typically encountered in airborne scenarios, has been investigated. These metrics tend to show that processings based on circular correlation (with either a matched or a reciprocal strategy), which have the most acceptable computational complexity, seem also to be the most resilient in presence of significant near clutter returns. These advantages may however be moderated by the substantial integration losses they induce to very distant targets. Ultimately, the best choice of correlation-based radar receiver is largely dictated by the scenario to be faced.

In any case, clutter mitigation was shown to be even more critical than in conventional radar due to the unusual pedestal component incurred by OFDM in the range-Doppler maps. It shall therefore be addressed in future work. A thorough detection performance analysis should also be conducted.

References

[1] Zhao, Q. and Sadler, B. M., "A survey of dynamic spectrum access," *IEEE Signal Process. Mag.*, vol. 24, no. 3, pp. 79–89, May 2007.

[2] Paul, B., Chiriyath, A. R., and Bliss, D. W., "Survey of RF communications and sensing convergence research," *IEEE Access*, vol. 5, pp. 252–270, 2017.

[3] Blunt, S. D. and Perrins, E. S., Eds., *Radar and Communication Spectrum Sharing*. Scitech Pub., 2018.

[4] *IEEE Trans. Aerosp. Electron. Syst. (Special Issue on Spectrum Sharing)*, vol. 55, no. 3, Jun. 2019.

[5] Griffiths, H. D. and Long, N. R. W., "Television-based bistatic radar," *IEE Proc. F - Commun., Radar and Signal Process.*, vol. 133, no. 7, pp. 649–657, Dec. 1986.

[6] Howland, P. E., Maksimiuk, D., and Reitsma, G., "FM radio based bistatic radar," *IEE Proc. Radar Sonar Navig.*, vol. 152, no. 3, pp. 107–115, Jun. 2005.

[7] Poullin, D., "Passive detection using digital broadcasters (DAB, DVB) with COFDM modulation," *IEE Proc. Radar Sonar Navig.*, vol. 152, no. 3, pp. 143–152, Jun. 2005.

[8] Tan, D. K. P., Sun, H., Lu, Y., Lesturgie, M., and Chan, H. L., "Passive radar using global system for mobile communication signal: theory, implementation and measurements," *IEE Proc. Radar Sonar Navig.*, vol. 152, no. 3, pp. 116–123, Jun. 2005.

[9] Salah, A., Abdullah, R. R., Ismail, A., Hashim, F., and Aziz, N. A., "Experimental study of LTE signals as illuminators of opportunity for passive bistatic radar applications," *IET Electron. Lett.*, vol. 50, no. 7, pp. 545–547, 2014.

[10] Shaojian, X., Bing, C., and Ping, Z., "Radar-communication integration based on DSSS techniques," in *Int. Conf. Signal Process.*, vol. 4, Nov. 2006.

[11] Saddik, G. N., Singh, R. S., and Brown, E. R., "Ultra-wideband multifunctional communications/radar system," *IEEE Trans. Microw. Theory Tech.*, vol. 55, no. 7, pp. 1431–1437, Jul. 2007.

[12] Sturm, C. and Wiesbeck, W., "Waveform design and signal processing aspects for fusion of wireless communications and radar sensing," *Proc. IEEE*, vol. 99, no. 7, pp. 1236–1259, Jul. 2011.

[13] Li, Y. G. and Stuber, G. L., *Orthogonal frequency division multiplexing for wireless communications*. Springer Science & Business Media, 2006.

[14] *Radio Broadcasting Systems; Digital Audio Broadcasting (DAB) to mobile, portable and fixed receivers*, ETSI EN 300 401 Std.

[15] *Digital Video Broadcasting (DVB); Framing structure, channel coding and modulation for digital terrestrial television*, ETSI EN 300 744 Std.

[16] *LTE: Evolved Universal Terrestrial Radio Access (E-UTRA), physical channels and modulation*, ETSI TS 136 211 Std.

[17] Berger, C. R., Demissie, B., Heckenbach, J., Willett, P., and Zhou, S., "Signal processing for passive radar using OFDM waveforms," *IEEE J. Sel. Topics Signal Process.*, vol. 4, no. 1, pp. 226–238, Feb. 2010.

[18] van Genderen, P. and Nikookar, H., "Radar network communication," in *Proc. Commun.*, Jun. 2006, pp. 313–316.

[19] Sturm, C., Sit, Y. L., Braun, M., and Zwick, T., "Spectrally interleaved multi-carrier signals for radar network applications and multi-input multi-output radar," *IET Radar Sonar Navig.*, vol. 7, no. 3, pp. 261–269, Mar. 2013.

[20] Sturm, C., Zwick, T., Wiesbeck, W., and Braun, M., "Performance verification of symbol-based OFDM radar processing," in *IEEE Radar Conf.*, May 2010, pp. 60–63.

[21] Sit, Y. L., Reichardt, L., Sturm, C., and Zwick, T., "Extension of the OFDM joint radar-communication system for a multipath, multiuser scenario," in *IEEE Radar Conf.*, May 2011, pp. 718–723.

[22] Palmer, J. E., Harms, H. A., Searle, S. J., and Davis, L., "DVB-T passive radar signal processing," *IEEE Trans. Signal Process.*, vol. 61, no. 8, pp. 2116–2126, Apr. 2013.

[23] Franken, G. E. A., Nikookar, H., and Genderen, P. V., "Doppler tolerance of OFDM-coded radar signals," in *Eur. Radar Conf.*, Sep. 2006, pp. 108–111.

[24] Sturm, C., Zwick, T., and Wiesbeck, W., "An OFDM system concept for joint radar and communications operations," in *Veh. Tech. Conf. Spring*, Apr. 2009, pp. 1–5.

[25] Searle, S., Palmer, J., Davis, L., O'Hagan, D. W., and Ummenhofer, M., "Evaluation of the ambiguity function for passive radar with OFDM transmissions," in *IEEE Radar Conf.*, May 2014, pp. 1040–1045.

[26] Gassier, G., Chabriel, G., Barrère, J., Briolle, F., and Jauffret, C., "A unifying approach for disturbance cancellation and target detection in passive radar using OFDM," *IEEE Trans. Signal Process.*, vol. 64, no. 22, pp. 5959–5971, Nov. 2016.

[27] Berthillot, C., Santori, A., Rabaste, O., Poullin, D., and Lesturgie, M., "DVB-T airborne passive radar: clutter block rejection," in *Int. Radar Conf.*, Sep. 2019.

[28] Mercier, S., Roque, D., and Bidon, S., "Study of the target self-interference in a low-complexity OFDM-based radar receiver," *IEEE Trans. Aerosp. Electron. Syst.*, vol. 55, no. 3, pp. 1200–1212, Jun. 2019.

[29] Chabriel, G., Barrere, J., Gassier, G., and Briolle, F., "Passive Covert Radars using CP-OFDM signals. A new efficient method to extract targets echoes," in *Int. Radar Conf.*, Oct. 2014, pp. 1–6.

[30] Roque, D. and Siclet, C., "Performances of weighted cyclic prefix OFDM with low-complexity equalization," *IEEE Commun. Lett.*, vol. 17, no. 3, pp. 439–442, Mar. 2013.

[31] Tigrek, R. F., Heij, W. J. A. D., and Genderen, P. V., "OFDM signals as the radar waveform to solve Doppler ambiguity," *IEEE Trans. Aerosp. Electron. Syst.*, vol. 48, no. 1, pp. 130–143, Jan. 2012.

[32] Glende, M., "PCL-signal-processing for sidelobe reduction in case of periodical illuminator signals," in *Int. Radar Symp.*, May 2006, pp. 1–4.

[33] Wojaczek, P., Colone, F., Cristallini, D., and Lombardo, P., "Reciprocal-filter-based STAP for passive radar on moving platforms," *IEEE Trans. Aerosp. Electron. Syst.*, vol. 55, no. 2, pp. 967–988, Apr. 2019.

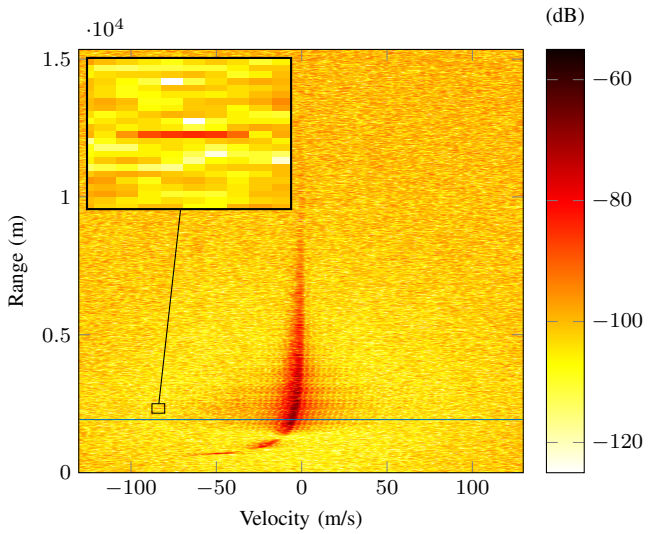

(a) MF $\chi^{(r,s)}$. Measured average background power: -99.83 dBW. Measured target peak: -84.98 dBW.

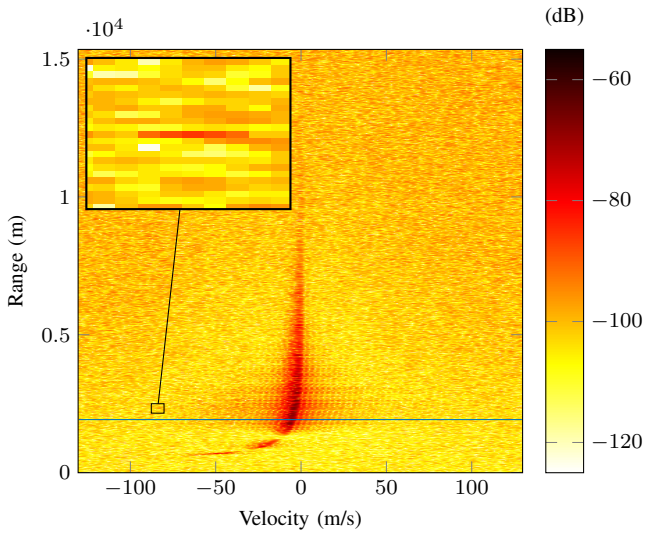

(b) PMF $\widetilde{\chi}^{(r,s)}$. Measured average background power: -99.35 dBW. Measured target peak: -86.66 dBW.

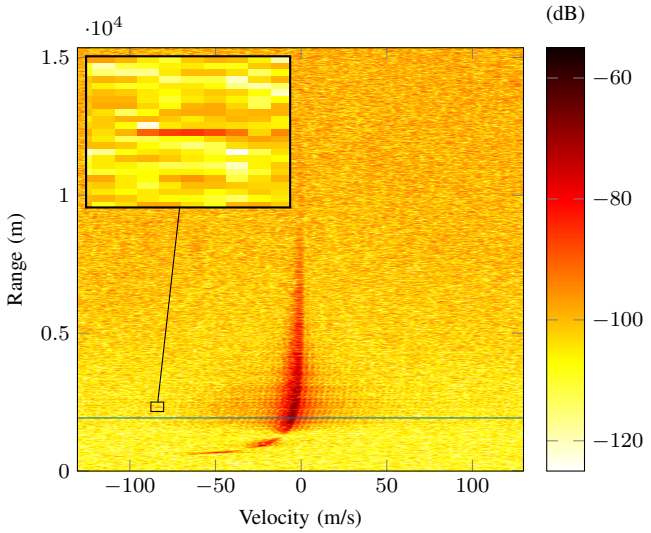

(c) PMF-CP $\widetilde{\chi}^{(\check{r},s)}$. Measured average background power: -99.14 dBW. Measured target peak: -86.43 dBW.

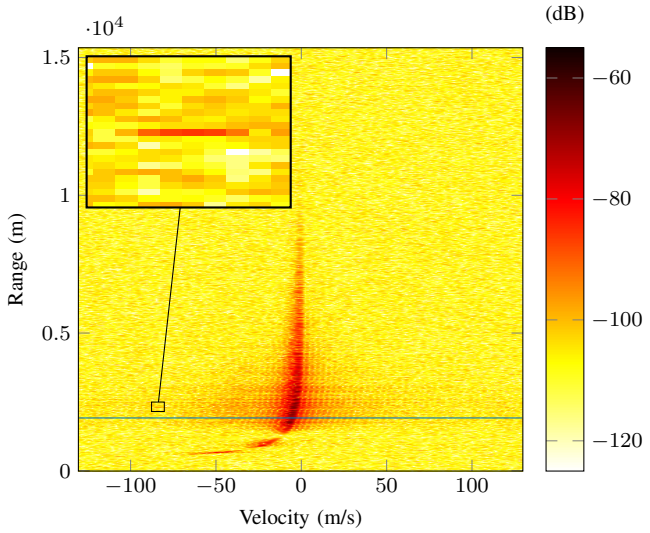

(d) PMF-CC $\widetilde{\chi}^{(\check{r},s_0)}$. Measured average background power: -106.01 dBW. Measured target peak: -86.23 dBW.

Fig. 5. Range-Doppler maps in presence of ground clutter after platform velocity compensation (the Doppler dimension is oversampled by a factor 4)

[34] Zhao, Z., Wan, X., Shao, Q., Gong, Z., and Cheng, F., "Multipath clutter rejection for digital radio mondiale-based HF passive bistatic radar with OFDM waveform," *IET Radar Sonar Navig.*, vol. 6, no. 9, pp. 867–872, Dec. 2012.

[35] Schwark, C. and Cristallini, D., "Advanced multipath clutter cancellation in OFDM-based passive radar systems," in *IEEE Radar Conf.*, May 2016, pp. 1–4.

[36] Searle, S., Gustainis, D., Hennessy, B., and Young, R., "Cancelling strong Doppler shifted returns in OFDM based passive radar," in *IEEE Radar Conf.*, Apr. 2018, pp. 0359–0354.

[37] Mercier, S., Bidon, S., Roque, D., and Enderli, C., "Clairvoyant clutter mitigation in a symbol-based OFDM radar receiver," in *Int. Radar Conf.*, Sep. 2019.

[38] Neeser, F. D. and Massey, J. L., "Proper complex random processes with applications to information theory," *IEEE Trans. Inf. Theory*, vol. 39, no. 4, pp. 1293–1302, 1993.

[39] Mercier, S., Roque, D., and Bidon, S., "Successive self-interference cancellation in a low-complexity WCP-OFDM radar receiver," in *Proc. IEEE Asilomar Conf. Signals, Syst. Comput.*, Oct. 2018, pp. 712–716.

[40] Brennan, L. E. and Reed, L. S., "Theory of adaptive radar," *IEEE Trans. Aerosp. Electron. Syst.*, vol. AES-9, no. 2, pp. 237–252, March 1973.

[41] Nathanson, F., Reilly, J., and Cohen, M., *Radar Design Principles: Signal Processing and the Environment*. Scitech Pub., 1999.

[42] Kemkemian, S., Nouvel-Fiani, M., Cornic, P., Bihan, P. L., and Garrec, P., "Radar systems for "sense and avoid" on UAV," in *Int. Radar Conf.*, Oct. 2009, pp. 1–6.

SECOND-ORDER MOMENTS OF THE RANGE-DOPPLER MAPS (FOR $M \gg 1$)

MF

$$\mathbb{E}\left\{|\chi^{(r,s)}[l,n]|^2\right\} \simeq \mathbb{E}\left\{|\alpha|^2\right\}\left[\sigma_c^4 KM\left|\mathcal{D}_K(l-l_0)\right|^2\left|\mathcal{D}_M(n_0-n)\right|^2\left|A^{(g,g)}\left(l-l_0,\frac{n_0-n}{LM}\right)\right|^2+\left(\mu_{c^4}-\sigma_c^4\right)\left|A^{(g,g)}\left(l-l_0,\frac{n_0-n}{LM}\right)\right|^2\right.$$
$$\left.+\sigma_c^4\left(\sum_{k\neq 0}\left|A^{(g,g)}\left(l-l_0,\frac{n_0-n}{LM}+\frac{k}{K}\right)\right|^2+\sum_k\left|A^{(g,g)}\left(l-l_0-\mathrm{sgn}(l-l_0)L,\frac{n_0-n}{LM}+\frac{k}{K}\right)\right|^2\right)\right]+\sigma^2\sigma_c^2 \tag{26a}$$

PMF

$$\mathbb{E}\left\{|\widetilde{\chi}^{(r,s)}[l,n]|^2\right\} \simeq \mathbb{E}\left\{|\alpha|^2\right\}\left[\sigma_c^4 KM\left|\mathcal{D}_K(l-l_0)\right|^2\left|\mathcal{D}_M(n_0-n)\right|^2\left|A^{(g,g)}_{\{l_0,\frac{n}{M}\}}\left(l-l_0,\frac{n_0}{LM}\right)\right|^2+\left(\mu_{c^4}-\sigma_c^4\right)\left|A^{(g,g)}_{\{l_0,\frac{n}{M}\}}\left(l-l_0,\frac{n_0}{LM}\right)\right|^2\right.$$
$$\left.+\sigma_c^4\left(\sum_{k\neq 0}\left|A^{(g,g)}_{\{l_0,\frac{n}{M}\}}\left(l-l_0,\frac{n_0}{LM}+\frac{k}{K}\right)\right|^2+\sum_k\left|A^{(g,g)}_{\{l_0,\frac{n}{M}\}}\left(l-l_0-\mathrm{sgn}(l-l_0)L,\frac{n_0}{LM}+\frac{k}{K}\right)\right|^2\right)\right]+\sigma^2\sigma_c^2 \tag{26b}$$

PMF-CP

$$\mathbb{E}\left\{|\widetilde{\chi}^{(\check{r},s)}[l,n]|^2\right\} \simeq \mathbb{E}\left\{|\alpha|^2\right\}\left[\sigma_c^4 KM\left|\mathcal{D}_K(l-l_0)\right|^2\left|\mathcal{D}_M(n_0-n)\right|^2\left|\dot{A}^{(\check{g},g)}_{\{l_0,\frac{n}{M}\}}\left(l-l_0,\frac{n_0}{LM}\right)\right|^2+\left(\mu_{c^4}-\sigma_c^4\right)\left|\dot{A}^{(\check{g},g)}_{\{l_0,\frac{n}{M}\}}\left(l-l_0,\frac{n_0}{LM}\right)\right|^2\right.$$
$$\left.+\sigma_c^4\left(\sum_{k\neq 0}\left|\dot{A}^{(\check{g},g)}_{\{l_0,\frac{n}{M}\}}\left(l-l_0,\frac{n_0}{LM}+\frac{k}{K}\right)\right|^2+\sum_k\left|\dot{A}^{(\check{g},g)}_{\{l_0,\frac{n}{M}\}}\left(l-l_0-\mathrm{sgn}(l-l_0)L,\frac{n_0}{LM}+\frac{k}{K}\right)\right|^2\right)\right]+\frac{L}{K}\sigma^2\sigma_c^2 \tag{26c}$$

PMF-CC

$$\mathbb{E}\left\{|\widetilde{\chi}^{(\check{r},s_0)}[l,n]|^2\right\} \simeq \mathbb{E}\left\{|\alpha|^2\right\}\left[\sigma_c^4 KM\left|\mathcal{D}_K(l-l_0)\right|^2\left|\mathcal{D}_M(n_0-n)\right|^2\left|A^{(g,\check{g})}\left(-l_0,\frac{n_0}{LM}\right)\right|^2+\left(\mu_{c^4}-\sigma_c^4\right)\left|A^{(g,\check{g})}\left(-l_0,\frac{n_0}{LM}\right)\right|^2\right.$$
$$\left.+\sigma_c^4\left(\sum_{k\neq 0}\left|A^{(g,\check{g})}\left(-l_0,\frac{n_0}{LM}+\frac{k}{K}\right)\right|^2+\sum_k\left|A^{(g,\check{g})}\left(-l_0+L,\frac{n_0}{LM}+\frac{k}{K}\right)\right|^2\right)\right]+\frac{L}{K}\sigma^2\sigma_c^2 \tag{26d}$$

RF

$$\mathbb{E}\left\{|\chi^{(r,\bar{s})}[l,n]|^2\right\} \simeq \mathbb{E}\left\{|\alpha|^2\right\}\left[KM\left|\mathcal{D}_K(l-l_0)\right|^2\left|\mathcal{D}_M(n_0-n)\right|^2\left|A^{(g,g)}\left(l-l_0,\frac{n_0-n}{LM}\right)\right|^2\right.$$
$$\left.+\sigma_c^2\sigma_{c^{-1}}^2\left(\sum_{k\neq 0}\left|A^{(g,g)}\left(l-l_0,\frac{n_0-n}{LM}+\frac{k}{K}\right)\right|^2+\sum_k\left|A^{(g,g)}\left(l-l_0-\mathrm{sgn}(l-l_0)L,\frac{n_0-n}{LM}+\frac{k}{K}\right)\right|^2\right)\right]+\sigma^2\sigma_{c^{-1}}^2 \tag{27a}$$

PRF

$$\mathbb{E}\left\{|\widetilde{\chi}^{(r,\bar{s})}[l,n]|^2\right\} \simeq \mathbb{E}\left\{|\alpha|^2\right\}\left[KM\left|\mathcal{D}_K(l-l_0)\right|^2\left|\mathcal{D}_M(n_0-n)\right|^2\left|A^{(g,g)}_{\{l_0,\frac{n}{M}\}}\left(l-l_0,\frac{n_0}{LM}\right)\right|^2\right.$$
$$\left.+\sigma_c^2\sigma_{c^{-1}}^2\left(\sum_{k\neq 0}\left|A^{(g,g)}_{\{l_0,\frac{n}{M}\}}\left(l-l_0,\frac{n_0}{LM}+\frac{k}{K}\right)\right|^2+\sum_k\left|A^{(g,g)}_{\{l_0,\frac{n}{M}\}}\left(l-l_0-\mathrm{sgn}(l-l_0)L,\frac{n_0}{LM}+\frac{k}{K}\right)\right|^2\right)\right]+\sigma^2\sigma_{c^{-1}}^2 \tag{27b}$$

PRF-CP

$$\mathbb{E}\left\{|\widetilde{\chi}^{(\check{r},\bar{s})}[l,n]|^2\right\} \simeq \mathbb{E}\left\{|\alpha|^2\right\}\left[KM\left|\mathcal{D}_K(l-l_0)\right|^2\left|\mathcal{D}_M(n_0-n)\right|^2\left|\dot{A}^{(\check{g},g)}_{\{l_0,\frac{n}{M}\}}\left(l-l_0,\frac{n_0}{LM}\right)\right|^2\right.$$
$$\left.+\sigma_c^2\sigma_{c^{-1}}^2\left(\sum_{k\neq 0}\left|\dot{A}^{(\check{g},g)}_{\{l_0,\frac{n}{M}\}}\left(l-l_0,\frac{n_0}{LM}+\frac{k}{K}\right)\right|^2+\sum_k\left|\dot{A}^{(\check{g},g)}_{\{l_0,\frac{n}{M}\}}\left(l-l_0-\mathrm{sgn}(l-l_0)L,\frac{n_0}{LM}+\frac{k}{K}\right)\right|^2\right)\right]+\frac{L}{K}\sigma^2\sigma_{c^{-1}}^2 \tag{27c}$$

PRF-CC

$$\mathbb{E}\left\{|\widetilde{\chi}^{(\check{r},\bar{s}_0)}[l,n]|^2\right\} \simeq \mathbb{E}\left\{|\alpha|^2\right\}\left[KM\left|\mathcal{D}_K(l-l_0)\right|^2\left|\mathcal{D}_M(n_0-n)\right|^2\left|A^{(g,\check{g})}\left(-l_0,\frac{n_0}{LM}\right)\right|^2\right.$$
$$\left.+\sigma_c^2\sigma_{c^{-1}}^2\left(\sum_{k\neq 0}\left|A^{(g,\check{g})}\left(-l_0,\frac{n_0}{LM}+\frac{k}{K}\right)\right|^2+\sum_k\left|A^{(g,\check{g})}\left(-l_0+L,\frac{n_0}{LM}+\frac{k}{K}\right)\right|^2\right)\right]+\frac{L}{K}\sigma^2\sigma_{c^{-1}}^2 \tag{27d}$$

Steven Mercier (S'17) was born in Fontenay-aux-Roses, France, in September 1994. He received the Dipl.Ing. degree and the M.S. degree in signal processing from Grenoble INP in 2017 and is now preparing a Ph.D. degree on waveform sharing for radar and communications at ISAE-SUPAERO, University of Toulouse, France.

Stéphanie Bidon (M'08–SM'20) received the Dipl.Ing. degree in aeronautics and the M.S. degree in signal processing from ENSICA, Toulouse, France, in 2004 and 2005, respectively, and the Ph.D. degree and the Habilitation à Diriger des Recherches in signal processing from INP, Toulouse, France, in 2008 and 2015, respectively.

She is currently a Professor with the Department of Electronics, Optronics and Signal at ISAE-SUPAERO, Toulouse, France. Her research interests include digital signal processing particularly with application to radar systems.

Damien Roque (M'15–SM'19) was born in Chambéry, France, in July 1986. He received the Dipl.Ing. degree in telecommunication engineering from the *École Nationale Supérieure des Télécommunications de Bretagne*, France, in 2009 and the Ph.D. in signal processing from Grenoble University, France, in 2012.

From 2012 to 2013, he was a temporary Assistant Professor at the *École Nationale Supérieure d'Informatique et de Mathématiques Appliquées de Grenoble*, France. He is now an Associate Professor at the *Institut Supérieur de l'Aéronautique et de l'Espace*, France. His research interests are in the area of spectrally efficient waveforms, including faster-than-Nyquist signaling, filtered multicarrier modulations, waveform sharing (radar/communication). He is an associate editor for IEEE Access, since 2019.

Cyrille Enderli received the M.S. degree in electrical engineering from the University of Lyon, France, in 2002 and the Ph.D. degree from the University of Marseille, France, in 2006.

Since then he has been an employee at Thales Defence Mission Systems in Elancourt, France, where his research interest have been in the areas of radar signal processing, adaptive detection, target identification, electronic warfare and machine learning.

He is a senior member of the SEE (Societe de l'Electricite, de l'Electronique et des technologies de l'information et de la communication).

APPENDIX A
RANGE-DOPPLER MAPS EXPRESSIONS IN A NOISE-FREE SINGLE TARGET SCENARIO

Herein we expand the derivations leading to (14a)–(14c). For its part, (14d) is easily deduced from its reciprocal version derived in [28].

1) Matched filter: Using successively (4)–(3)–(1), we obtain:

$$\begin{aligned}
\chi^{(r,s)}(l,\nu) &= \frac{1}{\sqrt{KM}} \sum_{p=0}^{LM-1} r[p]s^*[p-l]e^{-j2\pi\nu p/L} \\
&= \frac{\alpha}{\sqrt{KM}} \sum_{p=0}^{LM-1} s[p-l_0]s^*[p-l]e^{j2\pi(f_\mathrm{D}-\nu)p/L} \\
&= \frac{\alpha}{\sqrt{KM}} e^{j2\pi(f_\mathrm{D}-\nu)l_0/L} \sum_{p=-l_0}^{LM-l_0-1} s[p]s^*[p-(l-l_0)]e^{j2\pi(f_\mathrm{D}-\nu)p/L} \\
&= \frac{\alpha}{\sqrt{KM}} e^{j2\pi(f_\mathrm{D}-\nu)l_0/L} \sum_{k,m}\sum_{k',m'} c_{k,m}c^*_{k',m'} e^{j2\pi\frac{k'}{K}(l-l_0)} e^{-j2\pi\frac{km-k'm'}{K}L} \\
&\qquad \times \frac{1}{K} \sum_{p=-l_0}^{LM-l_0-1} g[p-mL]g^*[p-(l-l_0)-m'L]e^{j2\pi\left(\frac{f_\mathrm{D}-\nu}{L}+\frac{k-k'}{K}\right)p} \\
&= \frac{\alpha}{\sqrt{KM}} e^{j2\pi(f_\mathrm{D}-\nu)l_0/L} \sum_{k,m}\sum_{k',m'} c_{k,m}c^*_{k',m'} e^{j2\pi\frac{k'}{K}(l-l_0+(m'-m)L)} e^{j2\pi(f_\mathrm{D}-\nu)m} \\
&\qquad \times \frac{1}{K} \sum_{p=-l_0-mL}^{L(M-m)-l_0-1} g[p]g^*[p-(l-l_0+(m'-m)L)]e^{j2\pi\left(\frac{f_\mathrm{D}-\nu}{L}+\frac{k-k'}{K}\right)p}.
\end{aligned}$$

Given the support of g (2), the summation over p reduces to indices $p \in \{0,\dots,L-1\}$ only for $m \in \mathcal{I}_{M-1}$. Since we neglect the truncation of r, we instead presume it is true for all $m \in \mathcal{I}_M$, that is

$$\begin{aligned}
\chi^{(r,s)}(l,\nu) &\underset{M\gg 1}{\simeq} \frac{\alpha}{\sqrt{KM}} e^{j2\pi(f_\mathrm{D}-\nu)l_0/L} \sum_{k,m}\sum_{k',m'} c_{k,m}c^*_{k',m'} e^{j2\pi\frac{k'}{K}(l-l_0+(m'-m)L)} e^{j2\pi(f_\mathrm{D}-\nu)m} \\
&\qquad \times \frac{1}{K} \sum_{p=0}^{L-1} g[p]g^*[p-(l-l_0+(m'-m)L)]e^{j2\pi\left(\frac{f_\mathrm{D}-\nu}{L}+\frac{k-k'}{K}\right)p}.
\end{aligned} \tag{28}$$

By introducing the pulse-ambiguity function $A^{(g,g)}(l,f)$ (15) we finally get (14a).

2) Proximate matched filter: First, note that the PMF (7) can be rewritten as

$$\widetilde{\chi}^{(r,s)}(l,\nu) = \frac{1}{\sqrt{KM}} \sum_{p=0}^{LM-1} r[p]s^*[p-l]e^{-j2\pi\nu\lfloor\frac{p}{L}\rfloor}. \tag{29}$$

Following the same procedure as for the MF (*i.e.*, using successively (3), (1) and approximation (28)), we thus obtain

$$\begin{aligned}
\widetilde{\chi}^{(r,s)}(l,\nu) &\underset{M\gg 1}{\simeq} \frac{\alpha}{\sqrt{KM}} e^{j2\pi f_\mathrm{D} l_0/L} \sum_{k,m}\sum_{k',m'} c_{k,m}c^*_{k',m'} e^{j2\pi\frac{k'}{K}(l-l_0+(m'-m)L)} e^{j2\pi(f_\mathrm{D}-\nu)m} \\
&\qquad \times \frac{1}{K} \sum_{p=0}^{L-1} g[p]g^*[p-(l-l_0+(m'-m)L)]e^{j2\pi\left(\left(\frac{f_\mathrm{D}}{L}+\frac{k-k'}{K}\right)p-\nu\lfloor\frac{p+l_0}{L}\rfloor\right)} \\
&\underset{M\gg 1}{\simeq} \frac{\alpha}{\sqrt{KM}} e^{j2\pi f_\mathrm{D} l_0/L} \sum_{k,m}\sum_{k',m'} c_{k,m}c^*_{k',m'} e^{j2\pi\frac{k'}{K}(l-l_0+(m'-m)L)} e^{j2\pi(f_\mathrm{D}-\nu)m} \\
&\qquad \times \frac{1}{K} \left[\sum_{p=0}^{L-l_0-1} g[p]g^*[p-(l-l_0+(m'-m)L)]e^{j2\pi\left(\frac{f_\mathrm{D}}{L}+\frac{k-k'}{K}\right)p} \right. \\
&\qquad\qquad \left. + e^{-j2\pi\nu} \sum_{p=L-l_0}^{L-1} g[p]g^*[p-(l-l_0+(m'-m)L)]e^{j2\pi\left(\frac{f_\mathrm{D}}{L}+\frac{k-k'}{K}\right)p} \right]
\end{aligned} \tag{30}$$

since $\lfloor\frac{p+l_0}{L}\rfloor = 0$ if $p \in \{0,\dots,L-l_0-1\}$, and 1 if $p \in \{L-l_0,\dots,L-1\}$. Finally, introducing the improper pulse-ambiguity function (17) leads to (14b).

3) Proximate matched filter after CP-removal: As for the PMF, the PMF-CP (8) can be rewritten

$$\widetilde{\chi}^{(\check{r},s)}(l,\nu)=\frac{1}{\sqrt{KM}}\sum_{p=0}^{LM-1}\check{r}[p]s^*[p-l]e^{-j2\pi\nu\lfloor\frac{p}{L}\rfloor}.$$

As previously, we use successively (3), (1), (28) and (30), but this time $g[p]$ in (30) must be replaced by

$$\sqrt{\frac{L}{K}}g[p]\sum_{m_0}\check{g}[p+l_0-(m_0-m)L]=\begin{cases}\check{g}[p+l_0] & \text{if} \quad p\in\{0,\dots,L-l_0-1\}\\ \check{g}[p+l_0-L] & \text{if} \quad p\in\{L-l_0,\dots,L-1\}\end{cases} \tag{31}$$

given the definition of the pulses g (2) and $\check{g}$ (10). This gives

$$\begin{aligned}\widetilde{\chi}^{(\check{r},s)}(l,\nu)\underset{M\gg1}{\simeq}&\frac{\alpha}{\sqrt{KM}}e^{j2\pi f_{\mathrm{D}}l_0/L}\sum_{k,m}\sum_{k',m'}c_{k,m}c^*_{k',m'}e^{j2\pi\frac{k'}{K}(l-l_0+(m'-m)L)}e^{j2\pi(f_{\mathrm{D}}-\nu)m}\\&\times\frac{1}{K}\left[\sum_{p=0}^{L-l_0-1}\check{g}[p+l_0]g^*[p-(l-l_0+(m'-m)L)]e^{j2\pi\left(\frac{f_{\mathrm{D}}}{L}+\frac{k-k'}{K}\right)p}\right.\\&\left.+e^{-j2\pi\nu}\sum_{p=L-l_0}^{L-1}\check{g}[p+l_0-L]g^*[p-(l-l_0+(m'-m)L)]e^{j2\pi\left(\frac{f_{\mathrm{D}}}{L}+\frac{k-k'}{K}\right)p}\right]\end{aligned}$$

which boils down to (14c) after identifying the improper pulse-ambiguity function (18).

APPENDIX B
SECOND-ORDER MOMENTS OF THE RANGE-DOPPLER MAPS IN A NOISE-FREE SINGLE TARGET SCENARIO

Herein we detail the derivations of the expressions (26a) and (27a) in absence of noise. Extension to the rest of (26) and (27) is straightforward.

1) Matched filter: Based on the expression of the range-Doppler map we obtained for the MF (14a), we have

$$\begin{aligned}\mathbb{E}\left\{|\chi^{(r,s)}(l,\nu)|^2\right\}\underset{M\gg1}{\simeq}&\mathbb{E}\left\{|\alpha|^2\right\}\sum_{k_0,m_0}\sum_{k'_0,m'_0}\sum_{k_1,m_1}\sum_{k'_1,m'_1}\mathbb{E}\left\{c_{k_0,m_0}c^*_{k'_0,m'_0}c^*_{k_1,m_1}c_{k'_1,m'_1}\right\}\Psi_{k'_0,m_0,m'_0,l,\nu}\Psi^*_{k'_1,m_1,m'_1,l,\nu}\\&\times A^{(g,g)}\left(l-l_0+(m'_0-m_0)L,\frac{f_{\mathrm{D}}-\nu}{L}+\frac{k_0-k'_0}{K}\right)A^{(g,g)*}\left(l-l_0+(m'_1-m_1)L,\frac{f_{\mathrm{D}}-\nu}{L}+\frac{k_1-k'_1}{K}\right).\end{aligned}$$

Given the assumptions on the data symbols made in Section IV-A, $\mathbb{E}\left\{c_{k_0,m_0}c^*_{k'_0,m'_0}c^*_{k_1,m_1}c_{k'_1,m'_1}\right\}\neq0$ if and only if:

- Case 0: $(k'_1,m'_1)=(k_1,m_1)=(k'_0,m'_0)=(k_0,m_0)$ for which
$$\begin{aligned}\mathbb{E}\left\{c_{k_0,m_0}c^*_{k'_0,m'_0}c^*_{k_1,m_1}c_{k'_1,m'_1}\right\}&=\mathbb{E}\left\{|c_{k_0,m_0}|^4\right\}=\mu_{c^4}\\\Psi_{k'_0,m_0,m'_0,l,\nu}\Psi^*_{k'_1,m_1,m'_1,l,\nu}&=\frac{1}{KM}\end{aligned}$$
- Case 1: $[(k'_1,m'_1)=(k_1,m_1)]\neq[(k'_0,m'_0)=(k_0,m_0)]$ for which
$$\begin{aligned}\mathbb{E}\left\{c_{k_0,m_0}c^*_{k'_0,m'_0}c^*_{k_1,m_1}c_{k'_1,m'_1}\right\}&=\mathbb{E}\left\{|c_{k_0,m_0}|^2|c_{k_1,m_1}|^2\right\}=\mathbb{E}\left\{|c_{k_0,m_0}|^2\right\}\mathbb{E}\left\{|c_{k_1,m_1}|^2\right\}=\sigma_c^4\\\Psi_{k'_0,m_0,m'_0,l,\nu}\Psi^*_{k'_1,m_1,m'_1,l,\nu}&=\frac{1}{KM}e^{j2\pi\frac{k_0-k_1}{K}(l-l_0)}e^{j2\pi(f_{\mathrm{D}}-\nu)(m_0-m_1)}\end{aligned}$$
- Case 2: $[(k'_1,m'_1)=(k'_0,m'_0)]\neq[(k_1,m_1)=(k_0,m_0)]$ for which
$$\begin{aligned}\mathbb{E}\left\{c_{k_0,m_0}c^*_{k'_0,m'_0}c^*_{k_1,m_1}c_{k'_1,m'_1}\right\}&=\mathbb{E}\left\{|c_{k_0,m_0}|^2|c_{k'_0,m'_0}|^2\right\}=\mathbb{E}\left\{|c_{k_0,m_0}|^2\right\}\mathbb{E}\left\{|c_{k'_0,m'_0}|^2\right\}=\sigma_c^4\\\Psi_{k'_0,m_0,m'_0,l,\nu}\Psi^*_{k'_1,m_1,m'_1,l,\nu}&=\frac{1}{KM}.\end{aligned}$$

We therefore get

$$\mathbb{E}\left\{|\chi^{(r,s)}(l,\nu)|^2\right\}=\mathbb{E}\left\{|\alpha|^2\right\}\left(\mu_{c^4}\left|A^{(g,g)}\left(l-l_0,\frac{f_{\mathrm{D}}-\nu}{L}\right)\right|^2+\sigma_c^4\left|A^{(g,g)}\left(l-l_0,\frac{f_{\mathrm{D}}-\nu}{L}\right)\right|^2S_1+\sigma_c^4S_2\right) \tag{32}$$

where we set

$$S_1 \triangleq \frac{1}{KM}\sum_{k_0,m_0}\sum_{\substack{(k_1,m_1)\\ \neq(k_0,m_0)}} e^{j2\pi\frac{k_0-k_1}{K}(l-l_0)}e^{j2\pi(f_\mathrm{D}-\nu)(m_0-m_1)}$$

$$S_2 \triangleq \frac{1}{KM}\sum_{k_0,m_0}\sum_{\substack{(k_0',m_0')\\ \neq(k_0,m_0)}} \left|A^{(g,g)}\left(l-l_0+(m_0'-m_0)L, \frac{f_\mathrm{D}-\nu}{L}+\frac{k_0-k_0'}{K}\right)\right|^2.$$

On the one hand, we have S_1 that simplifies into

$$S_1 = \frac{1}{KM}\left(\sum_{k_0,m_0}\sum_{k_1,m_1} e^{j2\pi\frac{k_0-k_1}{K}(l-l_0)}e^{j2\pi(f_\mathrm{D}-\nu)(m_0-m_1)} - KM\right) = KM\left|\mathcal{D}_K(l-l_0)\right|^2\left|\mathcal{D}_M((f_\mathrm{D}-\nu)M)\right|^2 - 1 \quad (33)$$

and on the other hand, we have

$$\begin{aligned}
S_2 &= \frac{1}{KM}\sum_{k_0,m_0}\left(\sum_{k_0'\neq k_0}\left|A^{(g,g)}\left(l-l_0,\frac{f_\mathrm{D}-\nu}{L}+\frac{k_0-k_0'}{K}\right)\right|^2\right.\\
&\qquad\left.+\sum_{m_0'\neq m_0}\sum_{k_0'}\left|A^{(g,g)}\left(l-l_0+(m_0'-m_0)L,\frac{f_\mathrm{D}-\nu}{L}+\frac{k_0-k_0'}{K}\right)\right|^2\right)\\
&= \frac{1}{KM}\sum_{k_0}\left(\sum_{k_0'\neq k_0}\left|A^{(g,g)}\left(l-l_0,\frac{f_\mathrm{D}-\nu}{L}+\frac{k_0-k_0'}{K}\right)\right|^2\right.\\
&\qquad\left.+(M-1)\sum_{k_0'}\left|A^{(g,g)}\left(l-l_0-\mathrm{sgn}(l-l_0)L,\frac{f_\mathrm{D}-\nu}{L}+\frac{k_0-k_0'}{K}\right)\right|^2\right)\\
&= \sum_{k\neq 0}\left|A^{(g,g)}\left(l-l_0,\frac{f_\mathrm{D}-\nu}{L}+\frac{k}{K}\right)\right|^2 + \frac{M-1}{M}\sum_{k}\left|A^{(g,g)}\left(l-l_0-\mathrm{sgn}(l-l_0)L,\frac{f_\mathrm{D}-\nu}{L}+\frac{k}{K}\right)\right|^2 \qquad (34)
\end{aligned}$$

owing to the limited support of the pulse g (2) (*i.e.*, $g[p]=0$ if $p\notin\{0,\dots,L-1\}$) and to the K-periodicity in frequency of the pulse-ambiguity function $A^{(g,g)}(l,f)$ (15). Remark that the second sum in S_2 reduces to 0 in the target range bin $l=l_0$. Finally, injecting (33) and (34) in (32) while considering critical sampling in Doppler (*i.e.*, $\nu=n/M$) directly yields the expression in (26a) under our assumption $M\gg 1$.

2) Reciprocal filter: Considering this time the reciprocal version of (14a), we get:

$$\begin{aligned}
\mathbb{E}\left\{\left|\chi^{(r,\bar{s})}(l,\nu)\right|^2\right\} = \mathbb{E}\left\{|\alpha|^2\right\}&\sum_{k_0,m_0}\sum_{k_0',m_0'}\sum_{k_1,m_1}\sum_{k_1',m_1'}\mathbb{E}\left\{\frac{c_{k_0,m_0}c^*_{k_1,m_1}}{c_{k_0',m_0'}c^*_{k_1',m_1'}}\right\}\Psi_{k_0',m_0,m_0',l,\nu}\Psi^*_{k_1',m_1,m_1',l,\nu}\\
&\times A^{(g,g)}\left(l-l_0+(m_0'-m_0)L,\frac{f_\mathrm{D}-\nu}{L}+\frac{k_0-k_0'}{K}\right)A^{(g,g)^*}\left(l-l_0+(m_1'-m_1)L,\frac{f_\mathrm{D}-\nu}{L}+\frac{k_1-k_1'}{K}\right).
\end{aligned}$$

The case study for the expectation operator is the same as for the MF, namely $\mathbb{E}\left\{\frac{c_{k_0,m_0}c^*_{k_1,m_1}}{c_{k_0',m_0'}c^*_{k_1',m_1'}}\right\}\neq 0$ if and only if:

- Case 0: $(k_1',m_1')=(k_1,m_1)=(k_0',m_0')=(k_0,m_0)$ for which $\mathbb{E}\left\{\frac{c_{k_0,m_0}c^*_{k_1,m_1}}{c_{k_0',m_0'}c^*_{k_1',m_1'}}\right\}=1$.
- Case 1: $[(k_1',m_1')=(k_1,m_1)]\neq[(k_0',m_0')=(k_0,m_0)]$ for which $\mathbb{E}\left\{\frac{c_{k_0,m_0}c^*_{k_1,m_1}}{c_{k_0',m_0'}c^*_{k_1',m_1'}}\right\}=1$.
- Case 2: $[(k_1',m_1')=(k_0',m_0')]\neq[(k_1,m_1)=(k_0,m_0)]$ for which $\mathbb{E}\left\{\frac{c_{k_0,m_0}c^*_{k_1,m_1}}{c_{k_0',m_0'}c^*_{k_1',m_1'}}\right\}=\sigma_c^2\sigma^2_{c^{-1}}$.

This yields

$$\mathbb{E}\left\{\left|\chi^{(r,\bar{s})}(l,\nu)\right|^2\right\} = \mathbb{E}\left\{|\alpha|^2\right\}\left(\left|A^{(g,g)}\left(l-l_0,\frac{f_\mathrm{D}-\nu}{L}\right)\right|^2 + \left|A^{(g,g)}\left(l-l_0,\frac{f_\mathrm{D}-\nu}{L}\right)\right|^2 S_1 + \sigma_c^2\sigma^2_{c^{-1}}S_2\right)$$

where the expressions of S_1 and S_2 after simplification were found in (33) and (34). Once again, if considering critical sampling in Doppler (*i.e.*, $\nu=n/M$) as well as $M\gg 1$ we obtain (27a).

APPENDIX C
SECOND-ORDER MOMENTS OF THE RANGE-DOPPLER MAPS IN A NOISE-ONLY SCENARIO

Hereafter we derive the expressions of the noise power at the output of the MF, PMF and PMF-CP, reported in (26a)–(26c). Extension to their reciprocal counterparts (*i.e.*, RF, PRF and PRF-CP) (27a)–(27c) is straightforward. The cases of the PMF-CC (26d) and PRF-CC (27d) are deduced from [28].

1) Matched filter: Given (4), the noise component at the output of the MF is

$$\chi^{(w,s)}(l,\nu) \triangleq \frac{1}{\sqrt{KM}} \sum_{p=0}^{LM-1} w[p]s^*[p-l]e^{-j2\pi\nu p/L}$$

Since w is a white noise with variance σ^2 that is statistically independent from the data symbols, we get

$$\begin{aligned}
&\mathbb{E}\left\{|\chi^{(w,s)}(l,\nu)|^2\right\} \\
&= \frac{1}{KM}\sigma^2 \sum_{p=0}^{LM-1} \mathbb{E}\left\{|s^*[p-l]|^2\right\} \\
&= \frac{1}{KM}\sigma^2 \frac{1}{K} \sum_{p=0}^{LM-1} \sum_{k,m} \sum_{k',m'} \mathbb{E}\left\{c^*_{k,m}c_{k',m'}\right\} g^*[p-l-mL]g[p-l-m'L]e^{-j2\pi\frac{k}{K}(p-l-mL)}e^{j2\pi\frac{k'}{K}(p-l-m'L)} \\
&= \frac{1}{KM}\sigma^2\sigma_c^2 \sum_{k,m} \frac{1}{K} \sum_{p=0}^{LM-1} |g[p-l-mL]|^2 \\
&\underset{M\gg 1}{\simeq} \frac{1}{KM}\sigma^2\sigma_c^2 \sum_{k,m} \frac{1}{K} \sum_{p=0}^{L-1} |g[p]|^2 \\
&\underset{M\gg 1}{\simeq} \sigma^2\sigma_c^2
\end{aligned} \tag{35}$$

since we chose $\|g\|^2 = K$. The output noise power after critical sampling in Doppler is thus $\mathbb{E}\left\{|\chi^{(w,s)}[l,n]|^2\right\} = \sigma^2\sigma_c^2$.

2) Proximate matched filter: We re-express the output of the PMF as in (29). Regarding the noise we thus have

$$\widetilde{\chi}^{(w,s)}(l,\nu) \triangleq \frac{1}{\sqrt{KM}} \sum_{p=0}^{LM-1} w[p]s^*[p-l]e^{-j2\pi\nu\lfloor\frac{p}{L}\rfloor}.$$

Similarly as for the MF, we then get

$$\begin{aligned}
\mathbb{E}\left\{|\widetilde{\chi}^{(w,s)}(l,\nu)|^2\right\} &\underset{M\gg 1}{\simeq} \frac{1}{KM}\sigma^2\sigma_c^2 \sum_{k,m} \frac{1}{K} \sum_{p=0}^{L-1} |g[p]|^2 \\
&\underset{M\gg 1}{\simeq} \sigma^2\sigma_c^2.
\end{aligned} \tag{36}$$

After critical sampling in Doppler, the noise power at the output of the PMF is also $\mathbb{E}\left\{|\widetilde{\chi}^{(w,s)}[l,n]|^2\right\} = \sigma^2\sigma_c^2$.

3) Proximate matched filter after CP-removal: Similarly as with the PMF, the noise at the output of the PMF-CP is

$$\widetilde{\chi}^{(\breve{w},s)}(l,\nu) \triangleq \frac{1}{\sqrt{KM}} \sum_{p=0}^{LM-1} \breve{w}[p]s^*[p-l]e^{-j2\pi\nu\lfloor\frac{p}{L}\rfloor}.$$

We thus follow the same procedure that led to (35) and (36) except that one $g[p]$ must be replaced with

$$\frac{L}{K}g[p]\sum_{m_0}\breve{g}[p+l-(m_0-m)L]\sum_{m'_0}\breve{g}[p+l-(m'_0-m)L] = \frac{L}{K}\begin{cases}\breve{g}[p+l] & \text{if} \quad p\in\{0,\dots,L-l-1\}\\ \breve{g}[p+l-L] & \text{if} \quad p\in\{L-l,\dots,L-1\}\end{cases}$$

given (31) and the support of $\breve{g}$ (10), so that

$$\mathbb{E}\left\{|\widetilde{\chi}^{(\breve{w},s)}(l,\nu)|^2\right\} \underset{M\gg 1}{\simeq} \frac{L}{K}\sigma^2\sigma_c^2.$$

The noise critically sampled at the output of the PMF-CP has thus power $\mathbb{E}\left\{|\widetilde{\chi}^{(\breve{w},s)}[l,n]|^2\right\} = \frac{L}{K}\sigma^2\sigma_c^2$.